An Adaptive Threshold in Mammalian Neocortical Evolution

Eric Lewitus[1∞], Iva Kelava[1∞], Alex T. Kalinka[1],
Pavel Tomancak[1], and Wieland B Huttner[1*]

[1]Max Planck Institute of Molecular Cell Biology and Genetics, Pfotenhauerstr. 108, 01307 Dresden, Germany

[∞]These authors contributed equally

[*]Corresponding author

Abstract

Expansion of the neocortex is a hallmark of human evolution. However, it remains an open question what adaptive mechanisms facilitated its expansion. Here we show, using gyrencephaly index (GI) and other physiological and life-history data for 102 mammalian species, that gyrencephaly is an ancestral mammalian trait. We provide evidence that the evolution of a highly folded neocortex, as observed in humans, requires the traversal of a threshold of $\sim 10^9$ neurons, and that species above and below the threshold exhibit a bimodal distribution of physiological and life-history traits, establishing two phenotypic groups. We identify, using discrete mathematical models, a basal radial glia-derived transit-amplifying progenitor as evolutionarily necessary and sufficient for generating a fourteen-fold increase in daily prenatal neuron production and thus traversal of the neuronal threshold. We demonstrate that length of neurogenic period, rather than any novel progenitor-type, is sufficient to distinguish cortical neuron number between species within the same phenotypic group.

Introduction

Development of the human neocortex involves a lineage of neural stem and progenitor cells that forms a proliferative region along the ventricular epithelium. The proliferation of cells within this region expands the neocortex by increasing neuron number. At the onset of mammalian cortical neurogenesis, neuroepithelial cells transform into radially oriented apical radial glia (aRG), which proliferate extensively at the apical surface of the ventricular zone and divide asymmetrically to self-renew and generate a neuron, intermediate progenitor (IP), or basal radial glia (bRG) [1]. IP cells delaminate from the apical surface and translocate their nucleus to the basal region of the ventricular zone (VZ) to form a second germinal layer, the subventricular zone (SVZ), where they divide symmetrically to generate two neurons [2–4]. Similarly to aRG cells at the ventricular surface, bRG cells, which maintain a single fiber ascending only to the basal surface, divide asymmetrically [5–8]; but contrary to aRG cells, bRG in the human generate neurons via transit-amplifying progenitors (TAPs), a cell-type that is not observed to originate basally in the mouse [6]. The abventricular expansion of progenitors during cortical neurogenesis in humans further compartmentalizes the basal region into an inner and outer SVZ, driving the radial fibers to have divergent, rather than parallel, trajectories to the cortical plate, and thus creating the folded cortical pattern observed in gyrencephalic species through the tangential expansion of migrating neurons [9, 10]. For this reason, and based on supporting evidence obtained in the gyrencephalic human and ferret and lissencephalic mouse, it was originally thought that an abundance of bRG cells in the outer SVZ was an evolutionary determinant for establishing a relatively large and gyrencephalic neocortex [5, 6, 11]. But recent work in the lissencephalic marmoset (*Callithrix jacchus*) has shown that bRG cells may, in fact, exist in comparable abundance in both gyrencephalic and lissencephalic species [12, 13] and so cannot alone be sufficient for either establishing or increasing cortical gyrification. Thus, despite considerable progress in the study of brain size evolution [14–16], the adaptive mechanism that has evolved along certain mammalian lineages to produce a large and folded neocortex is not known.

In this study, we analyzed physiological and life-history data from 102 mammalian species (Table S1; Table S2; External Database 1). We show that a gyrencephalic neocortex is ancestral to all mammals (Fig. 1) and that GI (Fig. S1), like brain size, has increased and decreased along many mammalian lineages. These changes may be reliably characterized by convergent adaptations into two distinct physiological and life-history programs (Fig. 2a), resulting in a

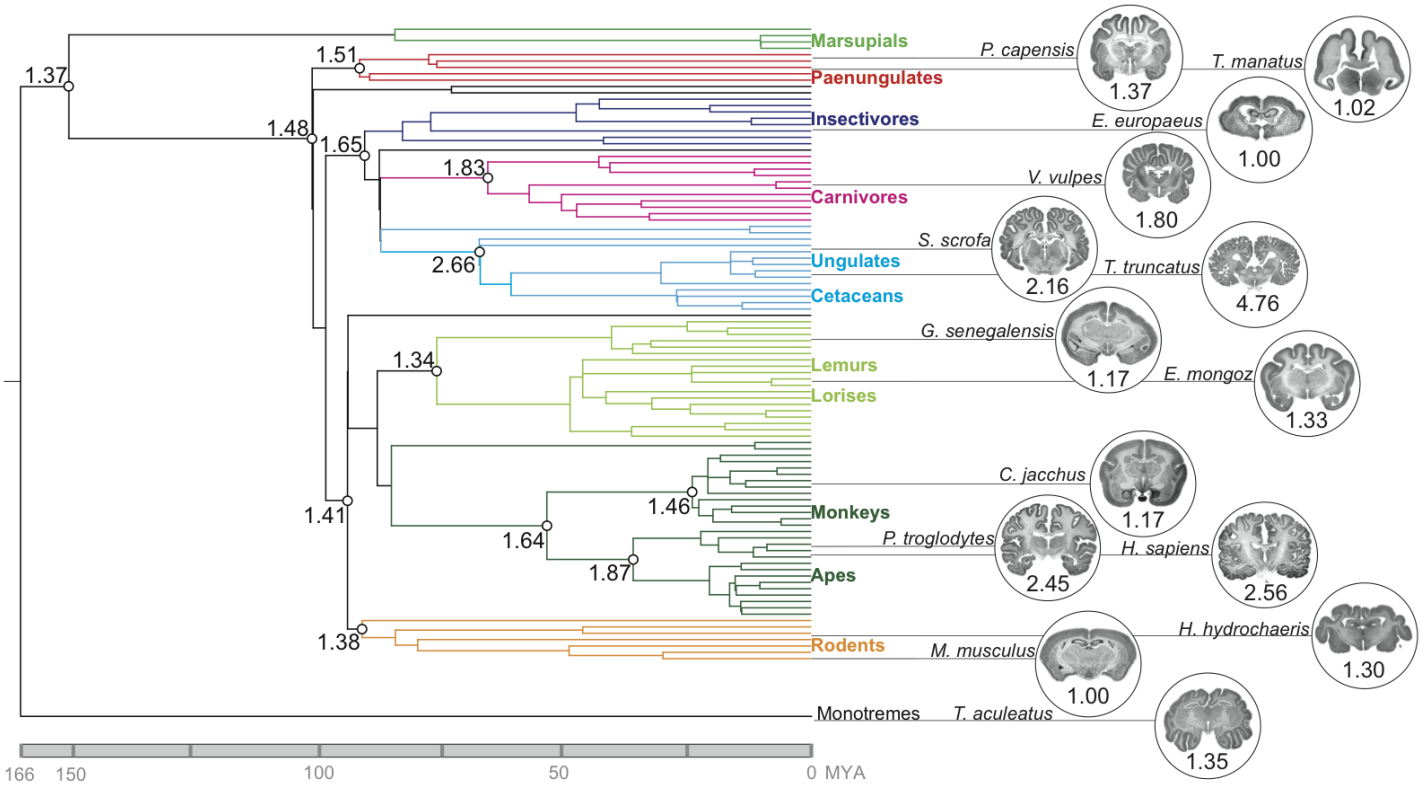

Figure 1: Ancestral reconstruction of GI values for 102 mammalian species. GI values were determined as illustrated in Fig. S1 for the species listed in Table S1. Reconstructed GI values for putative ancestors are presented at selected internal nodes of the phylogenetic tree. MYA, million years ago; colors indicate taxonomic groups. Images of Nissl-stained coronal sections of representative species for each taxonomic group, downloaded from http://brainmuseum.org, along with respective GI values, are shown on the right.

bimodal distribution of mammalian species (Fig. 2b) with a robust threshold value for both GI and neuron number (Fig. 3). Traversal of the threshold requires greater neuron production per gestation day (Fig. 4a,b), which we argue is necessitated by the evolution of bRG-derived TAPs during cortical neurogenesis (Fig. 5).

The mammalian ancestor was gyrencephalic

We tested multiple evolutionary models for GI evolution. The model that conferred most power to explain the GI values across the phylogeny while making the fewest assumptions about the data (i.e., had the lowest Akaike Information Criterion (AIC)) showed a disproportionate amount of evolutionary change to have occurred recently, rather than ancestrally, in mammals (Fig. S2) and diverged significantly from a null model of stochastic evolution [17]. We identified a folded neocortex (GI =1.37 $\pm$ 0.16 s.e.m.) as an ancestral mammalian trait (Fig. 1). It is apparent from ancestral and other internal node reconstructions (Fig. S3a,b) that GI is very

variable, but also that reductions in the rate at which GI evolves have favored branches leading to decreases in GI (e.g., strepsirrhines and insectivores) and accelerations in that rate have favored branches leading to increases in GI (e.g., carnivores and caviomorphs). A simulation of the average number of total evolutionary transitions between GI values evidences more affinity for transitioning from high-to-low than low-to-high GI values: the majority of high-to-low transitions (58.3%) occurred in species with a GI < 1.47; and the fewest transitions (16.7%) occurred across a threshold value of 1.5 (Fig. S4). This indicates that, although there is an evident trend in mammalian history to become increasingly gyrencephalic, the most variability in GI evolution has been concentrated among species below a certain threshold value (GI = 1.5). We therefore present a picture of early mammalian history, contrary to those previously painted, but which is gathering evidence through novel approaches [18, 19], that the Jurassic-era mammalian ancestor may, indeed, have been a large-brained species with a folded neocortex.

A threshold in cortical neuron number

The evolutionary effects of a folded neocortex on the behavior and biology of a species is not immediately clear. We therefore analyzed associations, across the phylogeny, of GI with discrete character states of 37 physiological and life-history traits (Table S2). Distinct sets of small but significant ($R^2 \leq 0.23$, $P < 0.03$) associations were found for species above and below a GI value of 1.5, indicating that these two groups of species adapt to their environments differently (Fig. 2a). Both groups were sampled from across the phylogeny, showing no phylogenetic signal. Clustering analyses also supported a bimodal distribution above and below a threshold value of 1.5 (Fig. 2b; Fig. S5). To test the bimodal distribution explicitly, we regressed GI values against neuroanatomical traits and found that each scaling relationship could be explained comparably well by either a non-linear function (Fig. 3a) or two grade-shifted linear functions, with the best-fit linear models drawing significantly different slopes ($P = 3.4 \times 10^{-4}$) for high-GI (> 1.5) and low-GI (< 1.5) species. (Fig. 3b,c). By plotting GI as a function of cortical neuron number, we were able to demarcate, with two significantly different linear regressions for high- and low-GI species ($T = 4.611$, d.f. $= 29$, $P = 2.8 \times 10^{-4}$), a cortical no-mans-land centered on an area approximating $1 \pm 0.11 \times 10^9$ neurons and 1.56 ± 0.06 GI (Fig. 3d). The deviation of these results from previous work, which have shown strong phylogenetic signals associated with both GI [20, 21] and neuron counts [22], may be explained by our more than 2-fold increase in sampled species. Variation in GI, therefore, has not evolved linearly across the phylogeny, but has in fact been differentially evolved in two phenotypic groups. Each group may be characterized not only by a high (> 1.5) or low (< 1.5) GI value, but also by a distinct constellation of other physiological and life-history traits which have accompanied each group

a

Trait	GI value			
	<1.31	1.31-1.47	1.64-2.94	>3
diurnality	P			
large litter size	P			
omnivory	P			
short maximum lifespan	P			
small body length	P			
small neonate brain weight	P			
leaves/branches/bark diet	P			
smallest body weight	P	P		
early age at eye opening	P	P		
early age at first breeding	P	P		
narrow habitat breadth	P	P		
nocturnality	P	P		N
short gestation length	P	P		
short juvenility	P	P		
short weaning period	P	P		
small brain weight	P	P		
small home range	P	P		
large population group size		P		
small litter size		P		
small social group size		P		
small weight at birth		P		
small weight at weaning		P		
vertebrate diet		P		
invertebrate diet		P		N
early female sexual maturity		P	P	
early male sexual maturity		P	P	
small interlitter interval		P	P	
fruit diet			P	
large home range			P	
medium body weight			P	
medium neonate brain weight			P	
moderate habitat breadth			P	
long maximum lifespan	N		P	P
large weight at birth	N		P	P
long juvenility		N	P	P
long weaning period			P	P
mixed activity timing			P	P
moderate age at first breeding			P	P
long gestation length			P	P
large social group size			P	P
large brain weight			P	P
medium interlitter interval				P
medium body length				P
late female sexual maturity				P
late male sexual maturity				P
wide habitat breadth				P
large body weight				P
large neonate brain weight				P

b

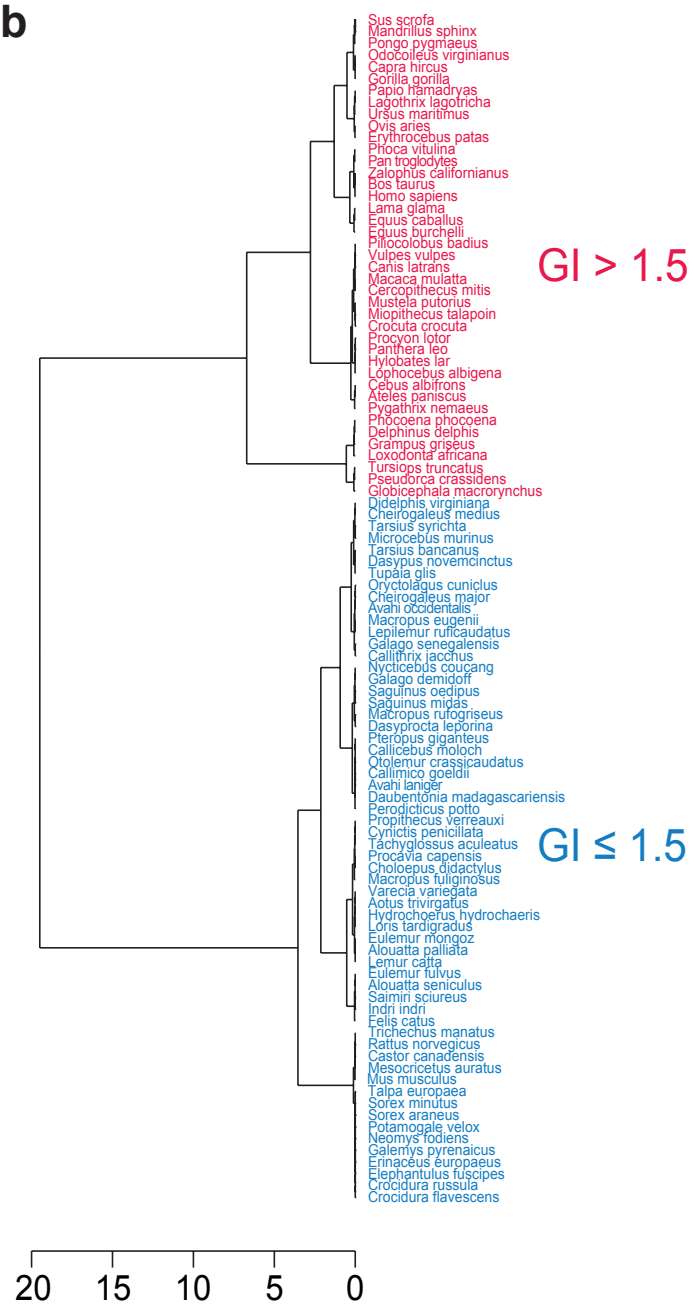

Figure 2: Clustering of GI values based on life-history association analysis (a) and minimum-energy distance (b).(a) Stochastic mapping of physiological and life-history traits with GI values for the 102 mammalian species listed in Table S1. GI values were separated into four groups based on clustering. Forty traits, each comprising 3 - 6 character states, were analyzed (see Table S2 for a complete list), and the states showing a significant positive (P, green) or negative (N, red) association with a group of GI values are shown. Note the major overlap between the two low-GI groups (10/27) and between the two high-GI groups (9/24), whereas only 3/48 character states are shared between GI groups ≤ 1.5 versus > 1.5. (b) Hierarchical clustering based on minimum-energy distance of the GI values for 101 mammalian species. Note that the greatest clustering height is between species with GI values of ≤ 1.5 and > 1.5.

over evolutionary time.

More efficient neurogenesis in large-brained species

By establishing an evolutionary threshold based on both degree of gyrencephaly and neuron number, we identified two neurogenic phenotypic groups, which found support in their distinct life-history associations (see previous section). These groups could be further divorced by accounting for the amount of brain weight accumulated per gestation day confident proxies for neonate brain weight and neurogenic period, respectively (Fig. S6) which we show to be, on average, 14-times greater in high- compared to low-GI species (Fig. 4). Notably, each GI group is constituted by both altricial and precocial species, so the degree of pre- versus post-natal development is not enough to explain the discrepancy in brain weight per gestation day in each group. Rather, to explain the discrepancy, we introduced a deterministic model of cortical neurogenesis, using series summarizing five neurogenic lineages and based on cell-cycle length, neuroepithelial founder pool size, neurogenic period, and estimates of relative progenitor-type population sizes (Table 1). We arrived at two models, based on the analysis of 16 species, that show the highest reliability for predicting cortical neuron numbers in a range of species: a mouse model, which implicates only aRG, IP, and bRG; and a human model, which additionally implicates proliferating bRG-derived TAPs. Each model is defined by the proportional occurrence of each lineage in that model (Table 2). Using the mouse model, with varying proportional occurrences of each lineage, we were able to predict neuron counts within 2% of the observed counts for low-GI species, but underestimated neuron counts by more than 80% in high-GI species (Fig. 5; Table S3). Similarly, the human model predicted neuron counts within 5% for high-GI species, but overestimated neuron counts by more than 150% for low-GI species. Increased proportional occurrences of the bRG lineage with increasing brain size was required to achieve estimates with $< 5\%$ deviation from observed neuron counts in low-GI species (Table 2; Fig. S7). Estimates of proportional occurrences in the mouse, marmoset, and rabbit are supported by previous work detailing relative abundances of different progenitor cell-types during cortical neurogenesis [8, 13], [IK and WBH, *in preparation*]. Evolutionary gain or loss of bRG-derived TAPs is an essential mechanistic determinant of neocortical expansion, such that its presence in high-GI species and absence in low-GI species is sufficient and even requisite for explaining neocortical evolution (Fig. S8).

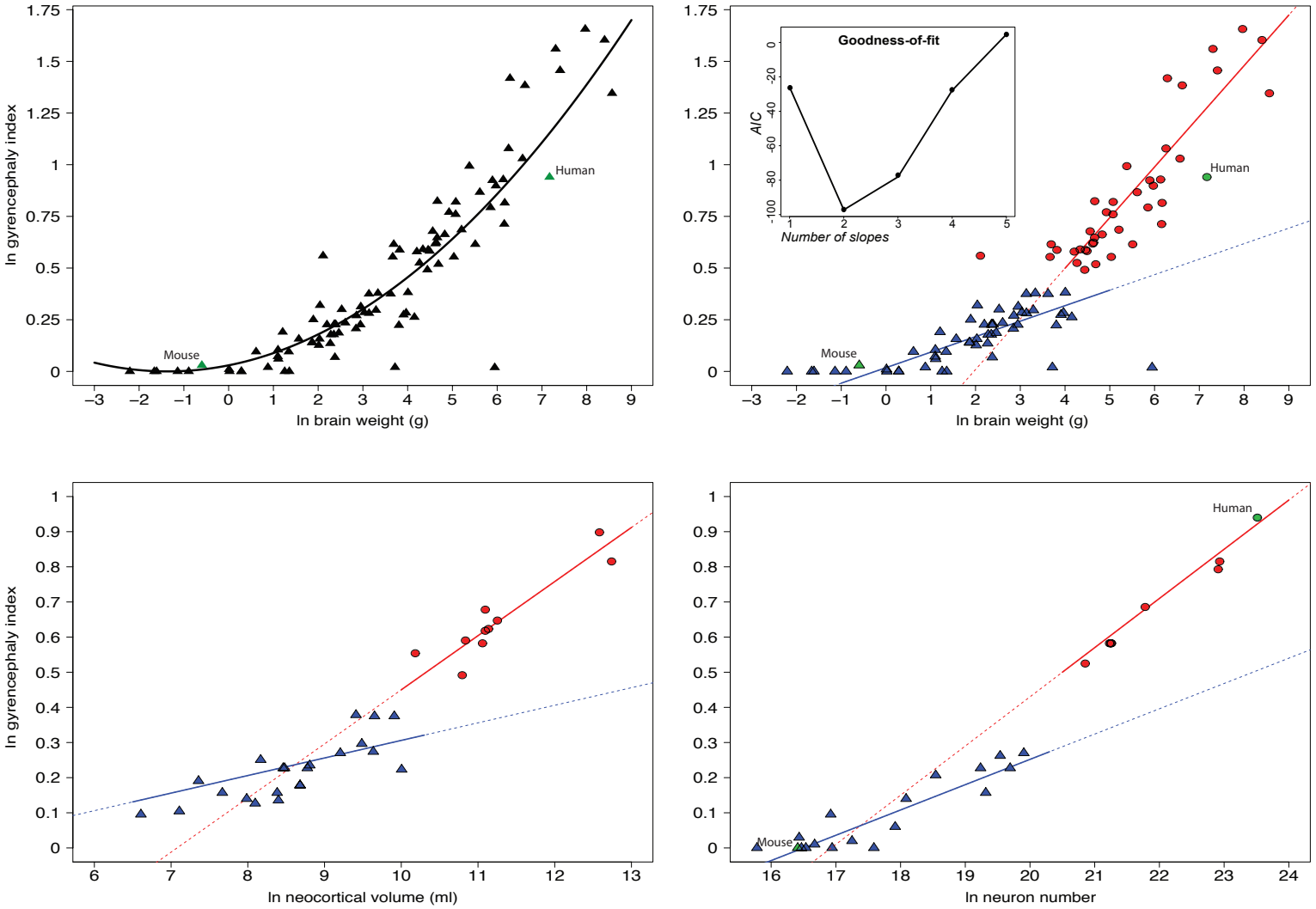

Figure 3: Ln-transformed plots showing GI values as a function of brain weight (a, b, 101 species), neocortical volume (c, 29 species) and cortical neuron number (d, 22 species). (a) Regression analysis using one non-linear fit for all values ($y = 0.018x^2 + 0.037x + 0.014$, $R^2 = 0.612$, $P = 6 \times 10^{-5}$); (b-d) regression analyses using two different linear functions (b, blue line: $y = 0.075x - 0.481$, $R^2 = 0.56$, $P = 4 \times 10^{-5}$, red line: $y = 0.245x + 0.018$, $R^2 = 0.73$, $P = 1 \times 10^{-5}$; c, blue line: $y = 0.050x - 0.194$, $R^2 = 0.21$, $P = 0.017$, red line: $y = 0.154x - 1.09$, $R^2 = 0.82$, $P = 0.004$; d, blue line: $y = 0.072x - 1.188$, $R^2 = 0.81$, $P = 1 \times 10^{-4}$; red line: $y = 0.140x - 2.370$, $R^2 = 0.98$, $P = 3 \times 10^{-5}$) for species with GI values of < 1.5 (blue triangles) and > 1.5 (red circles), respectively; mouse and human are indicated by green symbols. The inset in (b) shows the AIC values for models fitted with 1 – 5 linear slopes; note that a two-slope model best explains the data. See Table S1 for data.

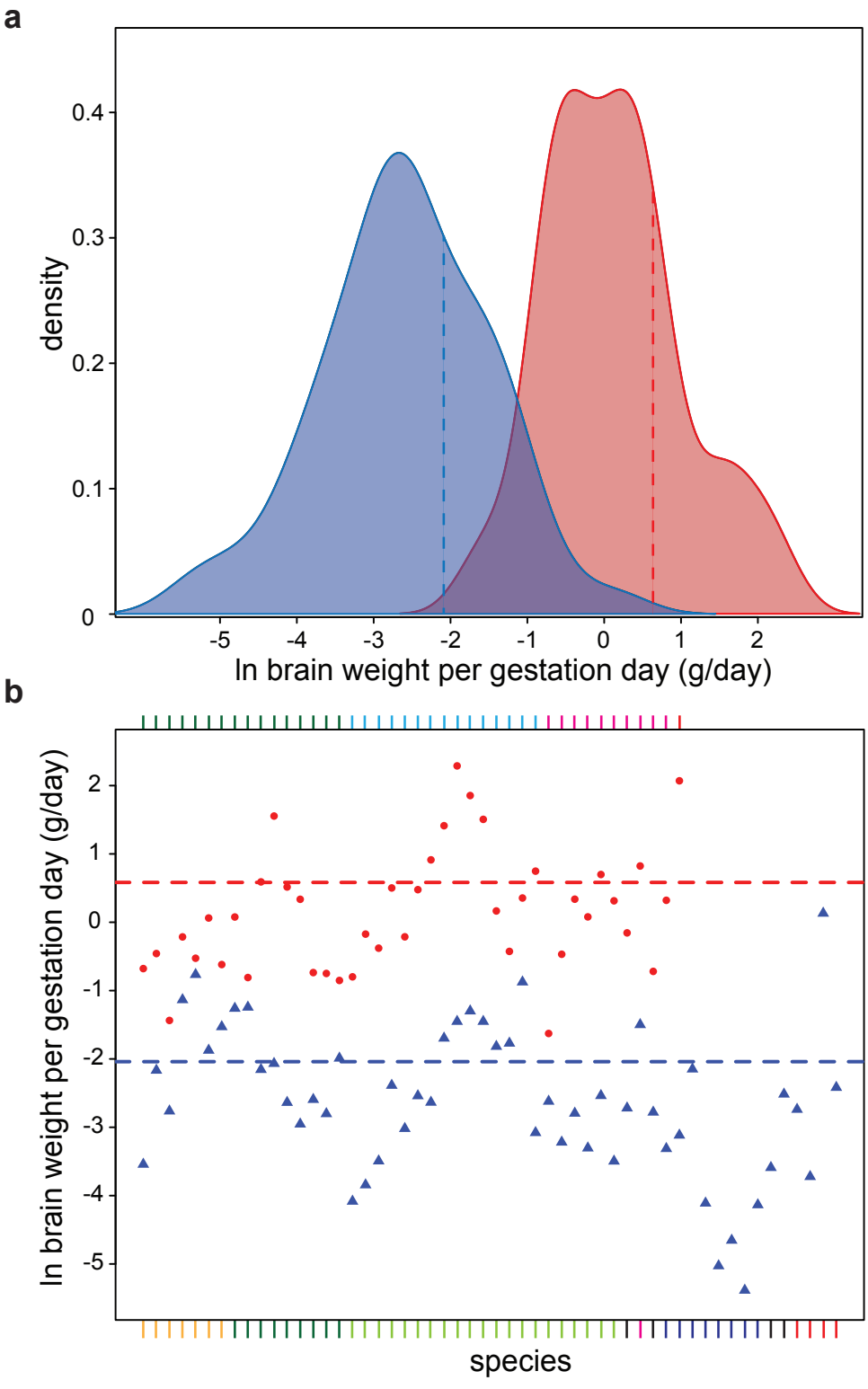

Figure 4: Brain weight per gestation day is considerably greater for high- versus low-GI species. (a) Ln-transformed density plot of brain weight per gestation day for 96 eutherian species listed in Table S1 with GI values of $\leq$ 1.5 (blue) and $>$ 1.5 (red). Note the significantly different means for the two groups (dashed blue and red lines, T = 5.16, d.f. = 41, P = 4×10^{-5}).(b) Ln-transformed plot of brain weight per gestation day for 96 mammalian species (see a). Dashed blue line, mean value for GI $\leq$ 1.5 (2.04 $\pm$ 0.047, s.d.); red dashed line, mean value for GI $>$ 1.5 (0.583 $\pm$ 0.050, s.d.). The colors in the index refer to species in Fig. 1. See Table S1 for data.

Adaptive evolution of a proliferative progenitor cell-type

To simulate the adaptiveness of evolving TAPs in two lissencephalic species - mouse and marmoset - we calculated trade-offs between neuroepithelial founder pool size and neurogenic period using mouse/marmoset and human models of cortical neurogenesis to achieve one billion neurons. We show that, in both species, evolving a lineage of bRG-derived TAPs is between 2- and 21-times more cost-efficient than either expanding founder pool size or lengthening neurogenesis; and that the marmoset, by evolving bRG-derived TAPs, could in fact reduce its observed founder pool size or neurogenic period to achieve one billion neurons (Fig. S9). We further clarified the significance of each progenitor-type with deterministic and stochastic models of temporal dynamics and progenitor cell-type variables. From these we conclude that basal progenitors are increasingly necessary in larger brains and that achieving 10^9 neurons is statistically implausible in the absence of bRG-derived TAPs (Table S4). Finally, we described the dynamics of TAPs, isolated from their observed lineage beginning at the apical surface, by introducing three ordinary differential equations (ODEs) modeling a self-renewing cell that generates either a differentiated cell or proliferative cell. We show that neuronal output of the system increases dramatically when both the initial pool of self-renewing cells and the likelihood of those initial cells to generate proliferative, rather than differentiated, cells approaches saturation (Fig. S10).

Discussion

The emergence of new structures, in the most general sense, is typically limited to selection on existing developmental processes; and conserved pathways may persist, over evolutionary time, even when the phenotype is transformed or unexpressed [23–25]. However, it is also evident that development may be adapted without affecting phenotype (e.g., [26, 27]). Therefore, in order to understand selective pressures acting on a discontinuous or convergent trait, it is necessary to investigate the underlying developmental processes generating it. We have shown that a gyrencephalic neocortex is ancestral to mammals, which is concordant with evidence [19] that the mammalian ancestor was large ($>$ 1kg) and long-lived ($>$ 25-year lifespan) and, furthermore, provides considerable resolution to recent evidence for a gyrencephalic eutherian ancestor [18] by sampling nearly twice as many species and categorizing gyrencephaly as a continuous, rather than a binary, trait. More surprisingly, we show that convergent evolution of higher-orders of gyrencephaly along divergent lineages has been accompanied by two distinct constellations of physiological and life-history paradigms. Specifically, species with a GI $>$ 1.5, which is commensurate with one billion cortical neurons, exhibit patterns of development and

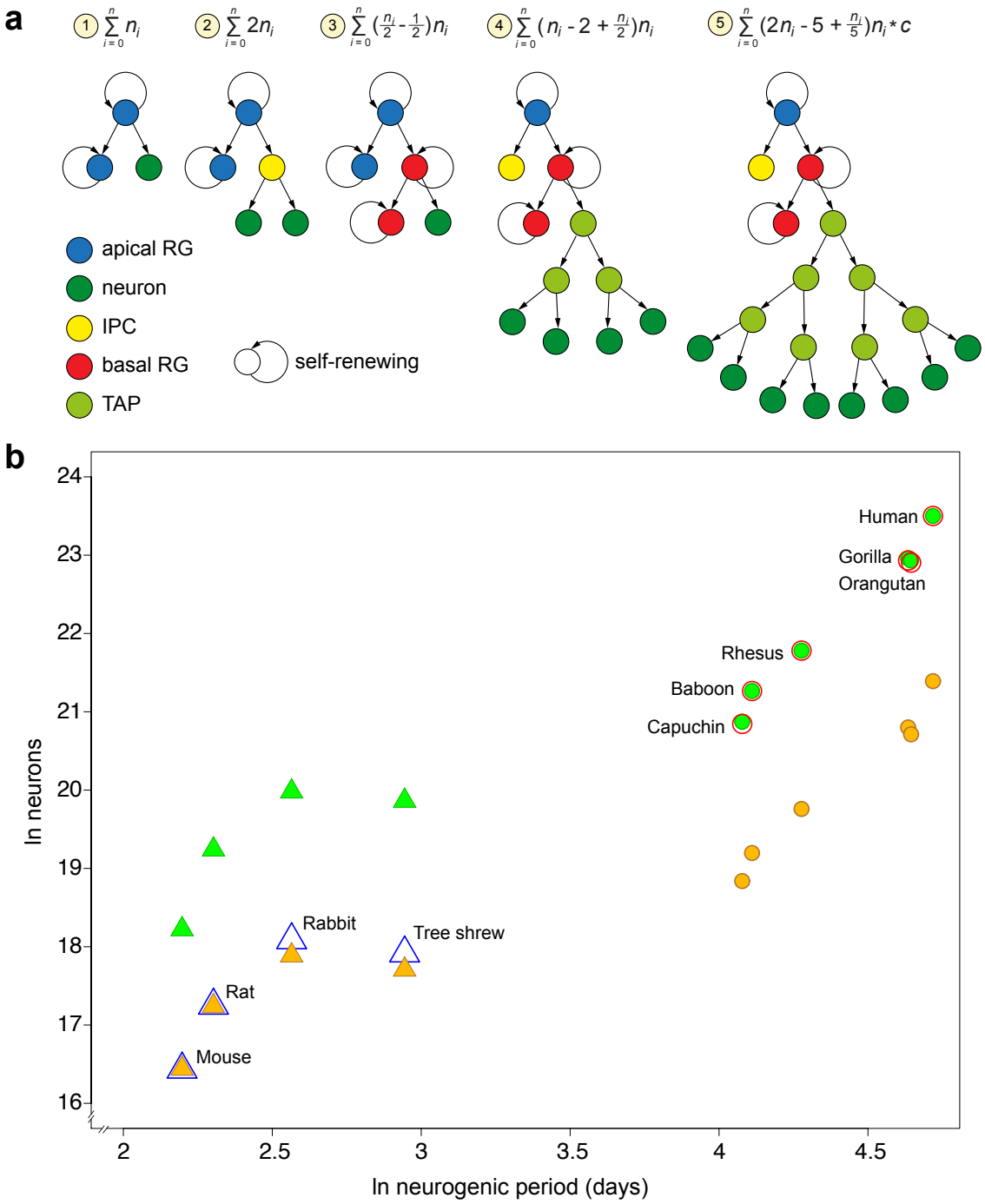

Figure 5: Distinct combinations of progenitor lineages are required to predict neocortical neuron numbers for low- versus high-GI species. (a) Schematic of the five progenitor lineages used in various combinations to predict neuron numbers. Series above the schematics summarize the neuronal output of each lineage, where n_i is the number of i divisions. A constant, c = 0.989, is incorporated into the series for lineage 5, allowing the series to converge on the true value of the lineage output as the number of divisions becomes increasingly numerous. (b) Ln-transformed plot of observed neuron counts as a function of neurogenic period for 4 species with a GI $\leq$ 1.5 (open blue triangles) and 6 species with a GI $>$ 1.5 (open red circles). Predicted neuron counts were calculated using combinations of the lineages in (a) that accurately fitted to the observed neuron counts either for mouse (closed gold symbols) or human (closed green symbols). Note that the mouse model implicates only lineages 1 – 3 and the human model only lineages 2 – 5. See Table 1 for observed and predicted neuron counts and Table 2 for the proportional contribution of each lineage for mouse and human.

life-history that are distinct from species with a GI < 1.5, irrespective of phylogeny. This implies that there is a considerable constraint on either the ability of species of a given neocortical size to exploit certain ecologies or the potential for species of a given ecology to freely adapt neocortical size. Furthermore, no species - with the exception of the house cat (*Felis catus*), which may be under unique selection pressures due to its ten-thousand-year-old domestication [28] - falls within the limits of the GI or neuronal threshold range (Fig. 3d). While our results countenance previous studies showing associations between physiological and life-history traits in mammals (see [29]), we identify those traits to have a bimodal distribution, rather than to vary allometrically, across species. This distribution depicts a Waddington-type landscape for neocortical expansion - albeit relevant at the species-level wherein the threshold represents an adaptive peak requiring a particular adaptation in neurogenic programming within a population for traversal. Our results may explain this landscape by mechanistic differences occurring during cortical neurogenesis between species above and below the threshold: the necessity of bRG-derived TAPs in high-GI species and their putative absence in low-GI species. The adaptation of bRG-derived TAPs may be tantamount to a relaxation of constraints along lineages leading to larger-brained species [30]. Furthermore, our human model clearly shows that the same neurogenic lineages in the same proportions are required to generate the neocortices of monkeys, apes, and humans, and may theoretically be extended to carnivores, artiodactlys, and other high-GI species, demonstrating that neurogenic period alone may be sufficient to explain differences in neocortical size between any species in the same GI group. If differences in neurogenesis among high-GI species can be largely explained by variation in neurodevelopmental timing, we may expect conservation at the genomic level in regions regulating that timing [31].

We propose that bRG-derived TAPs, rather than simply an abundance of bRG in an expanded SVZ, are necessary and sufficient for the evolution of an expanded and highly folded neocortex in mammals. We conclude that the inclusion of TAPs in the basal neurogenic program is the adaptive requirement for traversing an evolutionary threshold. But because we reconstruct the eutherian ancestor to have a GI value of 1.48 ± 0.13 (s.e.m.), which falls within the range of the observed threshold, we are left with an ambivalent evolutionary history for mammalian neocortical expansion: either (i) bRG-derived TAPs are ancestral to all eutherian mammals and were selected against along multiple lineages (e.g., rodents, strepsirrhinies), so that the ultimate loss of TAPs in certain taxa, and therefore the evolution of low-GI species, is the result of divergent developmental adaptations; or (ii) bRG-derived TAPs are not ancestral to eutherian mammals, but evolved convergently along multiple lineages, in which case the developmental process for their inclusion in neurogenic programming may be conserved, even if that process was unexpressed for long stretches of mammalian evolution. While both of these

histories are speculative, we have nonetheless revealed an important insight into mammalian evolution: neocortical expansion beyond a certain threshold requires a specific class of progenitor cell-type; and the difference in neurogenic programming between any species within the same GI group does not require novel progenitor-types or adaptations in progenitor-type behavior. Further research into the conservation of genomic regions regulating the expression of bRG-derived TAPs, either at the ventricle or through maintenance of a proliferative niche in the SVZ, in low- *versus* high-GI species may be sufficient to determine whether the mechanism for neocortical expansion has evolved independently in distantly related species or is the product of a deep homology in mammalian neurogenesis.

Materials and Methods

Calculating GI

We calculated GI using images of Nissl-stained coronal sections from http://brainmuseum.org. We used 10-22 sections, equally spaced along the anterior-posterior axis of the brain, for each species (Fig. S1). The inner and outer counters of the left hemisphere were traced in Fiji (http://fiji.sc/wiki/index.php/Fiji). The values calculated are marked with an asterisk in Table S1. Additional GI values were collected from the literature (Table S1; External Database 1). Work in humans and baboons has shown that inter-indvidual variation in GI is not enough to outweigh interspecific differences [32, 33].

Stochastic mapping of GI across the mammalian phylogeny

We used a comprehensive phylogenetic approach to map 41 life-history and physiological character traits collected from the literature (Tables S1,S2) onto hypotheses of phylogenetic relationships in Mammalia, in order to examine how those traits correlate, over evolutionary time, with degree of gyrencephaly. Continuous character traits were discretized using the consensus of natural distribution breaks calculated with a Jenks-Caspall algorithm [34], model-based clustering according to the Schwarz criterion [35], and hierarchical clustering [36]. Character histories were then corrected for body mass with a phylogenetic size correction [37] and summarized across the phylogeny using posterior probabilities. Associations between individual states of each character trait along those phylogenetic histories were calculated in SIMMAP (v1.5) using empirical priors [38]; the association between any two states was a measure of the frequency of occurrence (i.e., the amount of branch length across the tree) of those states on the phylogeny. The sums, rates, and types of changes for GI and body weight were plotted as

mutational maps to assess directional biases in their evolution [39–41]. The phylogeny used in this analysis was derived from a species-level supertree [42].

Reconstructing the evolutionary history of GI

Variation in the mode and tempo of a continuous character trait is not always best characterized by a random walk (i.e., Brownian motion). Therefore, we compared a range of evolutionary models on the phylogenetic distribution of GI to find the best fit for the data [43–46]. Log-likelihood scores for each model were tried against the random walk score using the cumulative distribution function of the χ^2 distribution. Maximum-likelihood ancestral character states of GI and rate-shifts in the evolution of GI were then constructed using the best-fit model, with the standard error and confidence intervals calculated from root node reconstruction in PDAP using independent contrasts [47–49]. To trace evolutionary changes in GI at individual nodes and along lineages, we used a two-rate mode that highlighted the differences in high (> 1) versus low (< 1) root-to-tip substitutions and then sampled rates based on posterior probabilities across the tree using a Monte Carlo Markov Chain. We assumed that transitioning between adjacent GI values had the highest likelihood of occurrence. The rate at a given node could then be compared to the rate at the subsequent node to determine if a rate transition was likely. We corroborated these results using the *auteur* package [50], which calculates rate-transitions at internal nodes under the assumption of an Ornstein-Uhlenbeck selection model [51] over one million Monte Carlo sampling iterations drawn from random samplings of posterior distributions of lineage-specific rates. Scaling relationships were determined for GI as a function of all continuous life-history and physiological traits, including adult cortical neuron counts. For three insectivore (*Sorex fumeus, Blarina brevicauda, Scalopus aquaticus*) species, data were available for neuron counts but not GI, and therefore we extrapolated the GI of those species based on their closest phylogenetic relatives. Finally, to test whether the bimodal distribution of GI may be influenced by the topology of the mammalian phylogenetic tree, we used an expectation-maximization algorithm. Each simulated trait was given the same variance as GI (Fig. S5) and the result was averaged over 10^4 simulated datasets. None of the simulations produced the same bimodal distribution of species observed for GI data.

Estimating neuroepithelial founder pool populations

We estimated neuroepithelial founder pool populations for mouse and human. For the mouse, we used coronal sections of an E11.5 mouse embryo obtained from the Allen Brain Atlas [52]. We obtained 19 sections equidistantly spaced along the anterior-posterior axis of the brain. The length of the ventricular surface of the dorsal telencephalon was manually traced in Fiji [53]

on each section starting from the point above the nascent hippocampus and ending in the point above the lateral ganglionic eminence. The horizontal length of the embryonic brain at E11.5 was measured with images from [54]. Using the coronal and horizontal measurements, we constructed a polygon representing the ventricular surface of the dorsal telencephalon and calculated the area of this surface in Fiji. We measured the surface area of the end-feet of neuroepithelial cells using EM images of the coronally cut apical surface of an E11.5 embryonic brain (Table S5). The diameter of a single cell was calculated by measuring the distance between the adherens junctions. We corroborated these end-feet calculations with published immunofluorescence stainings of the apical complex (ZO1 and N-cadherin) from an *en face* perspective [55, 56]. The average surface area of a single end-foot was calculated by approximating the end-foot as a hexagon; and the number of founder cells was estimated by dividing the surface of the dorsal telencephalon by the surface of an individual end-foot of the neuroepithelial cell, such that

$$\frac{Surfacearea(\mu m^2)}{2\pi(\frac{1}{2}Endfootdiameter(\mu m^2)}\frac{\sqrt{3}}{2} = founders \tag{1}$$

Our final mouse values were comparable to those previously published [57]. For the human, we followed the same procedure, using 10 coronal sections and one horizontal section of a gestation week (GW) 9 brain [58]. End-feet were calculated using EM images of the apical surface of a human brain at GW13. The measurements are available in Table S5. Because the number of founder cells per surface area was nearly equivalent in mouse and human (4 x 10^5/mm^2), we used this ratio, along with data on ventricular volume collected from the literature (Table S1; Table S2; External Database 1), to estimate neuroepithelial founder cell populations for a further 14 species (Table 1). For species where no data on ventricular volume were available, values were estimated based on a regression analysis against brain weight (Fig. S6b). Ventricular volume was then converted to surface area for each species by approximating the ventricle as a cylinder with a 4.5-to-1 height-to-diameter proportion. Ventricular volume-derived ventricular surface area estimates were corroborated with the surface areas calculated from the literature for mouse and human. Founder cell estimates were then computed based on the densities derived above for mouse and human. Using this method, but alternately ignoring our mouse and human calculations to define the parameters, we were able to predict mouse and human values within 10% of our calculations, respectively.

Mathematical modeling of neurogenesis

Workers have demonstrated the occurrence of three primary lineages of neuronal generation in mouse neurogenesis [59] and a further two lineages in human neurogenesis [6]. While there is evidence for at least one additional lineage in mouse [60], and further lineages may be speculated, we limited our model to the five that are considered to contribute most significantly to neuronal output [61–63]. The sequence of neuron generation in each of these five lineages was summarized in series and solved numerically (Fig. 5a). Neurogenic period was either taken from the literature (External Database 1) or estimated based on a regression analysis of neurogenic period as a function of gestation period (Fig. S6c). Neurogenic period in human was estimated using empirical observations from the literature [64–66]. The averaged cell-cycle length for apical and basal progenitors from the mouse (18.5 hours) was used for all non-primates [67]; averaged cell-cycle length for cortical areas 17 and 18 from the macaque (41 hours) was used for catarrhines [68]; an intermediary cell-cycle length (30 hours) was used for platyrrhines. Diminishing numbers of neuroepithelial cells have been observed to continue to proliferate at the ventricle until E18.5 in the mouse [4]. Therefore, final neuroepithelial founder pool estimates were calculated from the aforementioned by evenly decreasing the value of α in the Sherley equation [69] from 1 at E9.5 to 0 at E18.5 in the mouse and at comparable neurogenic stages in other species. Neuron numbers were calculated for each species from combinations of lineages. The proportional contribution of each lineage for each species was parameterized according to existing data on progenitor cell-type abundances in mouse [8], marmoset [13], and rabbit [IK and WBH, *in preparation*]. Where no such data were available, proportional contributions were permutated for all lineages until a best-fit estimate, based on cortical neuron numbers taken from the literature [22, 70–72], was achieved (Tables 1,2). Each lineage was assumed to occur from the first to final day of neurogenesis, although this is only approximately accurate. Finally, because of published estimates of postnatal apoptosis in the mammalian cortex [73–75], we assumed neuron counts to be 1.5-fold higher at the termination of neurogenesis than in the adult brain; therefore, neuron number at the termination of neurogenesis was estimated in each species by multiplying neuron numbers collected from the literature by 1.5. This multiplication is not represented in Table 1.

Calculating the effects of transit-amplifying progenitors on neuronal output

Trade-offs in adapting a human lineage combination with either an expanding neuroepithelial founder pool or lengthening neurogenic period were tested for the mouse (Mus musculus) and

marmoset (*Callithrix jacchus*), two lissencephalic species whose cell-type proportions during neurogenesis have been documented [8, 13, 60]. To estimate the relative reproductive value and stable-stage proportions of each of the lineages in the mouse and human models, we constructed a stage-structured Lefkovitch matrix, using sums of the lineage series (after 100 cycles) as fecundity values and complete permutations of the proportional contributions of each lineage as mortality values. The altered growth-rates of each lineage were calculated by excluding lineages one at a time and assuming 100% survival in the remaining lineages. We introduced three ODEs to explore the average dynamics of bRG-derived TAPs, such that: if a(t), b(t), and c(t) are the numbers of asymmetrically dividing cells, differentiated cells, and proliferative cells, respectively, then,

$$\frac{da}{dt} = 0 \tag{2}$$

$$\frac{db}{dt} = ra + 2rc \tag{3}$$

$$\frac{dc}{dt} = (1-r)a + (1-2r)c \tag{4}$$

where r is equal to growth-rate. If $a(t)$=a_0, then

$$b(t) = \frac{2r}{1-2r}(c_0 + \frac{1-r}{1-2r}a_0)(e^{(1-2r)t} - 1) - \frac{ra_0}{1-2r}t + b_0 \tag{5}$$

and

$$c(t) = (c_0 + \frac{1-r}{1-2r}a_0)e^{(1-2r)t} - \frac{ra_0}{1-2r}a_0 \tag{6}$$

We calculated the effect on neuronal output of increasing the likelihood of bRG-derived TAPs in the lineage (Fig. S10). The interdependent growth-rates in the model reflect a purely mechanistic interpretation of determining neuronal output from a finite pool of asymmetrically dividing cells. The ODEs, therefore, may not reflect differential regulation of neuronal output via direct versus indirect neurogenesis. The proliferative cells are designed to carry out one round of proliferation followed by a final round of self-consumption.

Author contributions: The project was conceived by EL, IK, ATK, and WBH; the mathematical models were formulated by EL; the dataset was compiled by IK; the data were analyzed by EL with support from ATK; the manuscript was written by EL with support from IK, ATK, PT,

and WBH.

Acknowledgments: We would like to thank Michaela Wilsch-Bruninger for providing electron microscopy data; and Michael Hiller, Yannis Kalaidzidis, Fong Kuan Wong, and Alex Sykes for helpful comments on the manuscript; and EL would like to thank Evan Charles for helpful discussion. IK was a member of the International Max Planck Research School for Molecular Cell Biology and Bioengineering and a doctoral student at the Technische Universitat Dresden. WBH was supported by grants from the Deutsche Forschungsgemeinschaft (DFG) (SFB 655, A2; TRR 83, Tp6) and the European Research Council (250197), by the DFG-funded Center for Regenerative Therapies Dresden, and by the Fonds der Chemischen Industrie.

Table 1: Parameters for models of cortical neurogenesis°

Species	*Gestation period (d)*	*Neurogenic period (d)†*	*Observed Neurons*	*Neuroepithelial founder pool (cells)†*	*Cell-cycle length (hours)*
Human	270	112	1.63E+10	3.10E+07	41
Gorilla	257	103*	9.10E+09	1.59E+07	41
Orangutan	260	104*	8.90E+09	1.16E+07	41
Macaque	166	60	1.71E+09	4.41E+06	41
Baboon	180	72*	2.88E+09	6.37E+06	41
Capuchin	158	59*	1.14E+09	2.97E+06	41
Owl monkey	138	55*	4.42E+08	1.05E+06	30
Callimico	153	60*	3.57E+08	6.92E+05	30
Marmoset	146	58	2.45E+08	6.71E+05	30
Galago	134	54*	2.26E+08	1.01E+06	30
Tree shrew	46	19*	6.04E+07	5.68E+05	18.5
Rabbit	30	13	7.15E+07	8.08E+05	18.5
Agouti	112	45*	1.10E+08	9.80E+05	18.5
Capybara	137	55*	3.10E+08	1.78E+06	18.5
Rat	21	10	3.10E+07	5.40E+05	18.5
Mouse	19	9	1.37E+07	3.99E+05	18.5

°*see External Database 1*

†see Materials and Methods

**estimate based on regression against gestation period (see Figure S6)*

Table 2: Best-fit proportional occurrences (%) of lineages in different taxa[œ]

Taxa	Lineage 1	Lineage 2	Lineage 3	Lineage 4	Lineage 5
Catarrhines	0	20	35	40	15
Capuchin	0	20	35	40	15
Owl monkey	0	50	50	0	0
Callimico	0	50	50	0	0
Marmoset[§]	0	60	40	0	0
Galago	0	75	25	0	0
Tree shrew	10	75	15	0	0
Rabbit[§]	10	75	15	0	0
Agouti	10	75	15	0	0
Capybara	10	75	15	0	0
Rat	10	80	10	0	0
Mouse[§]	10	80	10	0	0

[§] *supported by observational data (see Materials and Methods)*

[œ]*see Figure 5a*

References

[1] Santos J Franco and Ulrich Müller. Shaping our minds: stem and progenitor cell diversity in the mammalian neocortex. *Neuron*, 77(1):19–34, January 2013. ISSN 1097-4199. doi: 10.1016/j.neuron.2012.12.022. URL http://www.ncbi.nlm.nih.gov/pubmed/23312513. PMID: 23312513.

[2] S C Noctor, A C Flint, T A Weissman, R S Dammerman, and A R Kriegstein. Neurons derived from radial glial cells establish radial units in neocortex. *Nature*, 409(6821):714–720, February 2001. ISSN 0028-0836. doi: 10.1038/35055553. URL http://www.ncbi.nlm.nih.gov/pubmed/11217860. PMID: 11217860.

[3] Takaki Miyata, Ayano Kawaguchi, Kanako Saito, Masako Kawano, Tetsuji Muto, and Masaharu Ogawa. Asymmetric production of surface-dividing and non-surface-dividing cortical progenitor cells. *Development*, 131(13):3133–3145, July 2004. ISSN 0950-1991. doi: 10.1242/dev.01173. URL http://www.ncbi.nlm.nih.gov/pubmed/15175243. PMID: 15175243.

[4] Wulf Haubensak, Alessio Attardo, Winfried Denk, and Wieland B Huttner. Neurons arise in the basal neuroepithelium of the early mammalian telencephalon: a major site of neurogenesis. *Proceedings of the National Academy of Sciences of the United States of America*, 101(9):3196–3201, March 2004. ISSN 0027-8424. doi: 10.1073/pnas.0308600100. URL http://www.ncbi.nlm.nih.gov/pubmed/14963232. PMID: 14963232.

[5] Simone A Fietz, Iva Kelava, Johannes Vogt, Michaela Wilsch-Bräuninger, Denise Stenzel, Jennifer L Fish, Denis Corbeil, Axel Riehn, Wolfgang Distler, Robert Nitsch, and Wieland B Huttner. OSVZ progenitors of human and ferret neocortex are epithelial-like and expand by integrin signaling. *Nature Neuroscience*, 13(6):690–699, June 2010. ISSN 1546-1726. doi: 10.1038/nn.2553. URL http://www.ncbi.nlm.nih.gov/pubmed/20436478. PMID: 20436478.

[6] David V Hansen, Jan H Lui, Philip R L Parker, and Arnold R Kriegstein. Neurogenic radial glia in the outer subventricular zone of human neocortex. *Nature*, 464(7288):554–561, March 2010. ISSN 1476-4687. doi: 10.1038/nature08845. URL http://www.ncbi.nlm.nih.gov/pubmed/20154730. PMID: 20154730.

[7] Atsunori Shitamukai, Daijiro Konno, and Fumio Matsuzaki. Oblique radial glial divisions in the developing mouse neocortex induce self-renewing progenitors outside the germinal zone that resemble primate outer subventricular zone progenitors. *The Journal of Neuroscience*, 31(10):3683–3695, March 2011. ISSN 1529-2401. doi: 10.1523/JNEUROSCI.4773-10.2011. URL http://www.ncbi.nlm.nih.gov/pubmed/21389223. PMID: 21389223.

[8] Xiaoqun Wang, Jin-Wu Tsai, Bridget LaMonica, and Arnold R Kriegstein. A new subtype of progenitor cell in the mouse embryonic neocortex. *Nature Neuroscience*, 14(5):555–561, May 2011. ISSN 1097-6256. doi: 10.1038/nn.2807. URL http://dx.doi.org/10.1038/nn.2807.

[9] Iain H M Smart, Colette Dehay, Pascale Giroud, Michel Berland, and Henry Kennedy. Unique morphological features of the proliferative zones and postmitotic compartments of the neural epithelium giving rise to striate and extrastriate cortex in the monkey. *Cerebral Cortex*, 12(1):37–53, January 2002. ISSN 1047-3211. URL http://www.ncbi.nlm.nih.gov/pubmed/11734531. PMID: 11734531.

[10] Víctor Borrell and Isabel Reillo. Emerging roles of neural stem cells in cerebral cortex development and evolution. *Developmental Neurobiology*, 72(7):955–971, July 2012. ISSN 1932-846X. doi: 10.1002/dneu.22013. URL http://www.ncbi.nlm.nih.gov/pubmed/22684946. PMID: 22684946.

[11] Isabel Reillo, Camino de Juan Romero, Miguel Ángel García-Cabezas, and Víctor Borrell. A role for intermediate radial glia in the tangential expansion of the mammalian cerebral cortex. *Cerebral Cortex*, 21(7):1674–1694, July 2011. ISSN 1460-2199. doi: 10.1093/cercor/bhq238. PMID: 21127018.

[12] Fernando García-Moreno, Navneet A Vasistha, Nonata Trevia, James A Bourne, and Zoltán Molnár. Compartmentalization of cerebral cortical germinal zones in a lissencephalic primate and gyrencephalic rodent. *Cerebral Cortex*, 22(2):482–492, February 2012. ISSN 1460-2199. doi: 10.1093/cercor/bhr312. URL http://www.ncbi.nlm.nih.gov/pubmed/22114081. PMID: 22114081.

[13] Iva Kelava, Isabel Reillo, Ayako Y Murayama, Alex T Kalinka, Denise Stenzel, Pavel Tomancak, Fumio Matsuzaki, Cécile Lebrand, Erika Sasaki, Jens C Schwamborn, Hideyuki Okano, Wieland B Huttner, and Víctor Borrell. Abundant occurrence of basal radial glia in the subventricular zone of embryonic neocortex of a lissencephalic primate, the common marmoset callithrix jacchus. *Cerebral Cortex*, 22(2):469–481, February 2012. ISSN 1460-2199. doi: 10.1093/cercor/bhr301. PMID: 22114084.

[14] B L Finlay and R B Darlington. Linked regularities in the development and evolution of mammalian brains. *Science*, 268(5217):1578–1584, June 1995. ISSN 0036-8075. URL http://www.ncbi.nlm.nih.gov/pubmed/7777856. PMID: 7777856.

[15] Leah Krubitzer and Jon Kaas. The evolution of the neocortex in mammals: how is phenotypic diversity generated? *Current Opinion in Neurobiology*, 15(4):444–453, August 2005. ISSN 0959-4388. doi: 10.1016/j.conb.2005.07.003. URL http://www.ncbi.nlm.nih.gov/pubmed/16026978. PMID: 16026978.

[16] Reinmar Hager, Lu Lu, Glenn D Rosen, and Robert W Williams. Genetic architecture supports mosaic brain evolution and independent brain-body size regulation. *Nature Communications*, 3:1079, September 2012. ISSN 2041-1723. doi: 10.1038/ncomms2086. URL http://www.ncbi.nlm.nih.gov/pubmed/23011133. PMID: 23011133.

[17] M Pagel. Inferring the historical patterns of biological evolution. *Nature*, 401(6756):877–884, October 1999. ISSN 0028-0836. doi: 10.1038/44766. URL http://www.ncbi.nlm.nih.gov/pubmed/10553904. PMID: 10553904.

[18] Maureen A. O'Leary, Jonathan I. Bloch, John J. Flynn, Timothy J. Gaudin, Andres Giallombardo, Norberto P. Giannini, Suzann L. Goldberg, Brian P. Kraatz, Zhe-Xi Luo,

Jin Meng, Xijun Ni, Michael J. Novacek, Fernando A. Perini, Zachary S. Randall, Guillermo W. Rougier, Eric J. Sargis, Mary T. Silcox, Nancy B. Simmons, Michelle Spaulding, Paúl M. Velazco, Marcelo Weksler, John R. Wible, and Andrea L. Cirranello. The placental mammal ancestor and the Post–K-Pg radiation of placentals. *Science*, 339(6120):662 –667, February 2013. doi: 10.1126/science.1229237. URL http://www.sciencemag.org/content/339/6120/662.abstract.

[19] J Romiguier, V Ranwez, E J P Douzery, and N Galtier. Genomic evidence for large, long-lived ancestors to placental mammals. *Molecular Biology and Evolution*, 30(1):5–13, January 2013. ISSN 1537-1719. doi: 10.1093/molbev/mss211. URL http://www.ncbi.nlm.nih.gov/pubmed/22949523. PMID: 22949523.

[20] Praneshri Pillay and Paul R. Manger. Order-specific quantitative patterns of cortical gyrification. *European Journal of Neuroscience*, 25(9):2705–2712, May 2007. ISSN 1460-9568. doi: 10.1111/j.1460-9568.2007.05524.x. URL http://dx.doi.org/10.1111/j.1460-9568.2007.05524.x.

[21] Karl Zilles, Nicola Palomero-Gallagher, and Katrin Amunts. Development of cortical folding during evolution and ontogeny. *Trends in Neurosciences*, February 2013. ISSN 1878-108X. doi: 10.1016/j.tins.2013.01.006. URL http://www.ncbi.nlm.nih.gov/pubmed/23415112. PMID: 23415112.

[22] Frederico A C Azevedo, Ludmila R B Carvalho, Lea T Grinberg, José Marcelo Farfel, Renata E L Ferretti, Renata E P Leite, Wilson Jacob Filho, Roberto Lent, and Suzana Herculano-Houzel. Equal numbers of neuronal and nonneuronal cells make the human brain an isometrically scaled-up primate brain. *The Journal of Comparative Neurology*, 513(5):532–541, April 2009. ISSN 1096-9861. doi: 10.1002/cne.21974. URL http://www.ncbi.nlm.nih.gov/pubmed/19226510. PMID: 19226510.

[23] Ernst Mayr. The emegergence of evolutionary novelties. In *Evolution After Darwin*, pages 349–360. University of Chicago, 1960.

[24] N Shubin, C Tabin, and S Carroll. Fossils, genes and the evolution of animal limbs. *Nature*, 388(6643):639–648, August 1997. ISSN 0028-0836. doi: 10.1038/41710. URL http://www.ncbi.nlm.nih.gov/pubmed/9262397. PMID: 9262397.

[25] Brian K Hall. Descent with modification: the unity underlying homology and homoplasy as seen through an analysis of development and evolution. *Biological Reviews of the Cambridge Philosophical Society*, 78(3):409–433, August 2003. ISSN 1464-7931. URL http://www.ncbi.nlm.nih.gov/pubmed/14558591. PMID: 14558591.

[26] J. A. Bolker. Comparison of gastrulation in frogs and fish. *American Zoologist*, 34(3):313 –322, January 1994. doi: 10.1093/icb/34.3.313. URL http://icb.oxfordjournals.org/content/34/3/313.abstract.

[27] Alex T Kalinka and Pavel Tomancak. The evolution of early animal embryos: conservation or divergence? *Trends in Ecology & Evolution*, 27(7):385–393, July 2012. ISSN 0169-5347. doi: 10.1016/j.tree.2012.03.007. URL http://www.ncbi.nlm.nih.gov/pubmed/22520868. PMID: 22520868.

[28] Carlos A Driscoll, Juliet Clutton-Brock, Andrew C Kitchener, and Stephen J O'Brien. The taming of the cat. genetic and archaeological findings hint that wildcats became housecats earlier–and in a different place–than previously thought. *Scientific American*, 300(6): 68–75, June 2009. ISSN 0036-8733. URL http://www.ncbi.nlm.nih.gov/pubmed/19485091. PMID: 19485091.

[29] Robert D Martin, Michel Genoud, and Charlotte K Hemelrijk. Problems of allometric scaling analysis: examples from mammalian reproductive biology. *The Journal of Experimental Biology*, 208(Pt 9):1731–1747, May 2005. ISSN 0022-0949. doi: 10.1242/jeb.01566. URL http://www.ncbi.nlm.nih.gov/pubmed/15855404. PMID: 15855404.

[30] A. M. Boddy, M. R. McGowen, C. C. Sherwood, L. I. Grossman, M. Goodman, and D. E. Wildman. Comparative analysis of encephalization in mammals reveals relaxed constraints on anthropoid primate and cetacean brain scaling. *Journal of Evolutionary Biology*, 25(5):981–994, 2012. ISSN 1420-9101. doi: 10.1111/j.1420-9101.2012.02491.x. URL http://dx.doi.org/10.1111/j.1420-9101.2012.02491.x.

[31] Eric Lewitus and Alex T Kalinka. Neocortical development as an evolutionary platform for intragenomic conflict. *Frontiers in Neuroanatomy*, 7(2), 2013. ISSN 1662-5129. doi: 10.3389/fnana.2013.00002. URL http://www.ncbi.nlm.nih.gov/pubmed/23576960. PMID: 23576960.

[32] Jeffrey Rogers, Peter Kochunov, Karl Zilles, Wendy Shelledy, Jack Lancaster, Paul Thompson, Ravindranath Duggirala, John Blangero, Peter T Fox, and David C Glahn. On the genetic architecture of cortical folding and brain volume in primates. *Neuroimage*, 53(3):1103–1108, November 2010. ISSN 1095-9572. doi: 10.1016/j.neuroimage.2010.02.020. PMID: 20176115.

[33] Roberto Toro, Michel Perron, Bruce Pike, Louis Richer, Suzanne Veillette, Zdenka Pausova, and Tomáš Paus. Brain size and folding of the human cerebral cortex. *Cerebral Cortex*, 18(10):2352 –2357, October 2008. doi: 10.1093/cercor/bhm261. URL http://cercor.oxfordjournals.org/content/18/10/2352.abstract.

[34] G.F. Jenks and F.C. Caspall. Error on choroplethic maps: definition, measurement, reduction. *Annals of the Association of American Geographers*, 61:217–244, 1971.

[35] C. Fraley and A.E. Raftery. Model-Based clustering, discriminant analysis, and density estimation. *Journal of the American Statistical Association*, 97:611–631, 2002.

[36] G.J. Szekely and M.L. Rizzo. Hierarchical clustering via joint Between-Within distances: Extending ward's minimum variance method. *Journal of Classification*, 22:151–183, 2005.

[37] David C Collar and Peter C Wainwright. Discordance between morphological and mechanical diversity in the feeding mechanism of centrarchid fishes. *Evolution*, 60(12): 2575–2584, December 2006. ISSN 0014-3820. URL http://www.ncbi.nlm.nih.gov/pubmed/17263118. PMID: 17263118.

[38] Jonathan P Bollback. SIMMAP: stochastic character mapping of discrete traits on phylogenies. *BMC Bioinformatics*, 7:88, 2006. ISSN 1471-2105. doi: 10.1186/1471-2105-7-88. URL http://www.ncbi.nlm.nih.gov/pubmed/16504105. PMID: 16504105.

[39] C.W. Cunningham. Some limitations of ancestral Character-State reconstruction when testing evolutionary hypotheses. *Systematic Biology*, 48:665–674, 1999.

[40] John P Huelsenbeck and Bruce Rannala. Detecting correlation between characters in a comparative analysis with uncertain phylogeny. *Evolution*, 57(6):1237–1247, June 2003. ISSN 0014-3820. URL http://www.ncbi.nlm.nih.gov/pubmed/12894932. PMID: 12894932.

[41] E Lewitus and C Soligo. Life-History correlates of placental structure in eutherian evolution. *Evolutionary Biology*, 38(3):287–305, 2011.

[42] Olaf R P Bininda-Emonds, Marcel Cardillo, Kate E Jones, Ross D E MacPhee, Robin M D Beck, Richard Grenyer, Samantha A Price, Rutger A Vos, John L Gittleman, and Andy Purvis. The delayed rise of present-day mammals. *Nature*, 446(7135):507–512, March 2007. ISSN 1476-4687. doi: 10.1038/nature05634. URL http://www.ncbi.nlm.nih.gov/pubmed/17392779. PMID: 17392779.

[43] J Felsenstein. Maximum-likelihood estimation of evolutionary trees from continuous characters. *American Journal of Human Genetics*, 25(5):471–492, September 1973. ISSN 0002-9297. URL http://www.ncbi.nlm.nih.gov/pubmed/4741844. PMID: 4741844.

[44] Luke J Harmon, Jason T Weir, Chad D Brock, Richard E Glor, and Wendell Challenger. GEIGER: investigating evolutionary radiations. *Bioinformatics*, 24(1):129–131, January 2008. ISSN 1367-4811. doi: 10.1093/bioinformatics/btm538. URL http://www.ncbi.nlm.nih.gov/pubmed/18006550. PMID: 18006550.

[45] Brian C O'Meara, Cécile Ané, Michael J Sanderson, and Peter C Wainwright. Testing for different rates of continuous trait evolution using likelihood. *Evolution*, 60(5):922–933, May 2006. ISSN 0014-3820. URL http://www.ncbi.nlm.nih.gov/pubmed/16817533. PMID: 16817533.

[46] Emmanuel Paradis, Julien Claude, and Korbinian Strimmer. APE: analyses of phylogenetics and evolution in r language. *Bioinformatics*, 20(2):289–290, January 2004. ISSN 1367-4803. URL http://www.ncbi.nlm.nih.gov/pubmed/14734327. PMID: 14734327.

[47] Jr Garland, Theodore and Ives. Using the past to predict the present: Confidence intervals for regression equations in phylogenetic comparative methods. *The American Naturalist*, 155(3):346–364, March 2000. ISSN 1537-5323. doi: 10.1086/303327. URL http://www.ncbi.nlm.nih.gov/pubmed/10718731. PMID: 10718731.

[48] Jr Garland, Theodore, Albert F Bennett, and Enrico L Rezende. Phylogenetic approaches in comparative physiology. *The Journal of Experimental Biology*, 208(Pt 16):3015–3035, August 2005. ISSN 0022-0949. doi: 10.1242/jeb.01745. URL http://www.ncbi.nlm.nih.gov/pubmed/16081601. PMID: 16081601.

[49] WP Maddison and DR Maddison. Mesquite: a modular system for evolutionary analysis, 2011.

[50] Jonathan M Eastman, Michael E Alfaro, Paul Joyce, Andrew L Hipp, and Luke J Harmon. A novel comparative method for identifying shifts in the rate of character evolution on trees. *Evolution*, 65(12):3578–3589, December 2011. ISSN 1558-5646. doi: 10.1111/j.1558-5646.2011.01401.x. URL http://www.ncbi.nlm.nih.gov/pubmed/22133227. PMID: 22133227.

[51] M.A. Butler and A.A. King. Phylogenetic comparative analysis: a modeling approach for adaptive evolution. *The American Naturalist*, 164(6):683–695, 2004.

[52] Ed S Lein, Michael J Hawrylycz, Nancy Ao, Mikael Ayres, Amy Bensinger, Amy Bernard, Andrew F Boe, Mark S Boguski, Kevin S Brockway, Emi J Byrnes, Lin Chen, Li Chen, Tsuey-Ming Chen, Mei Chi Chin, Jimmy Chong, Brian E Crook, Aneta Czaplinska, Chinh N Dang, Suvro Datta, Nick R Dee, Aimee L Desaki, Tsega Desta, Ellen Diep, Tim A Dolbeare, Matthew J Donelan, Hong-Wei Dong, Jennifer G Dougherty, Ben J Duncan, Amanda J Ebbert, Gregor Eichele, Lili K Estin, Casey Faber, Benjamin A Facer, Rick Fields, Shanna R Fischer, Tim P Fliss, Cliff Frensley, Sabrina N Gates, Katie J Glattfelder, Kevin R Halverson, Matthew R Hart, John G Hohmann, Maureen P Howell, Darren P Jeung, Rebecca A Johnson, Patrick T Karr, Reena Kawal, Jolene M Kidney, Rachel H Knapik, Chihchau L Kuan, James H Lake, Annabel R Laramee, Kirk D Larsen, Christopher Lau, Tracy A Lemon, Agnes J Liang, Ying Liu, Lon T Luong, Jesse Michaels, Judith J Morgan, Rebecca J Morgan, Marty T Mortrud, Nerick F Mosqueda, Lydia L Ng, Randy Ng, Geralyn J Orta, Caroline C Overly, Tu H Pak, Sheana E Parry, Sayan D Pathak, Owen C Pearson, Ralph B Puchalski, Zackery L Riley, Hannah R Rockett, Stephen A Rowland, Joshua J Royall, Marcos J Ruiz, Nadia R Sarno, Katherine Schaffnit, Nadiya V Shapovalova, Taz Sivisay, Clifford R Slaughterbeck, Simon C Smith, Kimberly A Smith, Bryan I Smith, Andy J Sodt, Nick N Stewart, Kenda-Ruth Stumpf, Susan M Sunkin, Madhavi Sutram, Angelene Tam, Carey D Teemer, Christina Thaller, Carol L Thompson, Lee R Varnam, Axel Visel, Ray M Whitlock, Paul E Wohnoutka, Crissa K Wolkey, Victoria Y Wong, Matthew Wood, Murat B Yaylaoglu, Rob C Young, Brian L Youngstrom, Xu Feng Yuan, Bin Zhang, Theresa A Zwingman, and Allan R Jones. Genome-wide atlas of gene expression in the adult mouse brain. *Nature*, 445 (7124):168–176, January 2007. ISSN 1476-4687. doi: 10.1038/nature05453. URL http://www.ncbi.nlm.nih.gov/pubmed/17151600. PMID: 17151600.

[53] Johannes Schindelin, Ignacio Arganda-Carreras, Erwin Frise, Verena Kaynig, Mark Longair, Tobias Pietzsch, Stephan Preibisch, Curtis Rueden, Stephan Saalfeld, Benjamin Schmid, Jean-Yves Tinevez, Daniel James White, Volker Hartenstein, Kevin Eliceiri, Pavel Tomancak, and Albert Cardona. Fiji: an open-source platform for biological-image analysis. *Nature Methods*, 9(7):676–682, July 2012. ISSN 1548-7105. doi: 10.1038/nmeth.2019. URL http://www.ncbi.nlm.nih.gov/pubmed/22743772. PMID: 22743772.

[54] Gill Bejerano, Craig B Lowe, Nadav Ahituv, Bryan King, Adam Siepel, Sofie R Salama, Edward M Rubin, W James Kent, and David Haussler. A distal enhancer and an ultracon-

served exon are derived from a novel retroposon. *Nature*, 441(7089):87–90, May 2006. ISSN 1476-4687. doi: 10.1038/nature04696. URL http://www.ncbi.nlm.nih.gov/pubmed/16625209. PMID: 16625209.

[55] Ronald S. Bultje, David R. Castaneda-Castellanos, Lily Yeh Jan, Yuh-Nung Jan, Arnold R. Kriegstein, and Song-Hai Shi. Mammalian par3 regulates progenitor cell asymmetric division via notch signaling in the developing neocortex. *Neuron*, 63(2):189–202, July 2009. ISSN 0896-6273. doi: doi:10.1016/j.neuron.2009.07.004. URL http://www.sciencedirect.com/science/article/pii/S0896627309005066.

[56] Véronique Marthiens and Charles ffrench-Constant. Adherens junction domains are split by asymmetric division of embryonic neural stem cells. *EMBO reports*, 10(5):515–520, May 2009. ISSN 1469-3178. doi: 10.1038/embor.2009.36. URL http://www.ncbi.nlm.nih.gov/pubmed/19373255. PMID: 19373255.

[57] Tarik F. Haydar, Richard S. Nowakowski, Paul J. Yarowsky, and Bruce K. Krueger. Role of founder cell deficit and delayed neuronogenesis in microencephaly of the trisomy 16 mouse. *The Journal of Neuroscience*, 20(11):4156 –4164, June 2000. URL http://www.jneurosci.org/content/20/11/4156.abstract.

[58] Shirley Ann Bayer and Joseph Altman. *Atlas of Human Central Nervous System Development: The human brain during the later first trimester*. CRC Press, Florida, 2006.

[59] Simone A Fietz and Wieland B Huttner. Cortical progenitor expansion, self-renewal and neurogenesis-a polarized perspective. *Current Opinion in Neurobiology*, 21(1):23–35, February 2011. ISSN 1873-6882. doi: 10.1016/j.conb.2010.10.002. URL http://www.ncbi.nlm.nih.gov/pubmed/21036598. PMID: 21036598.

[60] Stephen C Noctor, Verónica Martínez-Cerdeño, Lidija Ivic, and Arnold R Kriegstein. Cortical neurons arise in symmetric and asymmetric division zones and migrate through specific phases. *Nature Neuroscience*, 7:136–144, January 2004. ISSN 1097-6256. doi: 10.1038/nn1172. URL http://www.nature.com/doifinder/10.1038/nn1172.

[61] Pasko Rakic. Evolution of the neocortex: a perspective from developmental biology. *Nature Reviews Neuroscience*, 10(10):724–735, October 2009. ISSN 1471-0048. doi: 10.1038/nrn2719. PMID: 19763105.

[62] Jan H. Lui, David V. Hansen, and Arnold R. Kriegstein. Development and evolution of the human neocortex. *Cell*, 146(1):18–36, July 2011. ISSN 00928674. doi: 10.1016/j.cell.2011.06.030. URL http://linkinghub.elsevier.com/retrieve/pii/S0092867411007057.

[63] Zoltán Molnár. Evolution of cerebral cortical development. *Brain, Behavior and Evolution*, 78(1):94–107, 2011. ISSN 1421-9743. doi: 10.1159/000327325. URL http://www.ncbi.nlm.nih.gov/pubmed/21691047. PMID: 21691047.

[64] Irina Bystron, Pasko Rakic, Zoltán Molnár, and Colin Blakemore. The first neurons of the human cerebral cortex. *Nature Neuroscience*, 9(7):880–886, July 2006. ISSN 1097-6256. doi: 10.1038/nn1726. PMID: 16783367.

[65] Brian Howard, Yanhui Chen, and Nada Zecevic. Cortical progenitor cells in the developing human telencephalon. *Glia*, 53(1):57–66, January 2006. ISSN 0894-1491. doi: 10.1002/glia.20259. PMID: 16158418.

[66] Sabrina Malik, Govindaiah Vinukonda, Linnea R Vose, Daniel Diamond, Bala B R Bhimavarapu, Furong Hu, Muhammad T Zia, Robert Hevner, Nada Zecevic, and Praveen Ballabh. Neurogenesis continues in the third trimester of pregnancy and is suppressed by premature birth. *Journal of Neuroscience*, 33(2):411–423, January 2013. ISSN 1529-2401. doi: 10.1523/JNEUROSCI.4445-12.2013. PMID: 23303921.

[67] Yoko Arai, Jeremy N Pulvers, Christiane Haffner, Britta Schilling, Ina Nüsslein, Federico Calegari, and Wieland B Huttner. Neural stem and progenitor cells shorten s-phase on commitment to neuron production. *Nature Communications*, 2:154, January 2011. ISSN 2041-1723. doi: 10.1038/ncomms1155. URL http://www.ncbi.nlm.nih.gov/pubmed/21224845. PMID: 21224845.

[68] Agnès Lukaszewicz, Pierre Savatier, Véronique Cortay, Pascale Giroud, Cyril Huissoud, Michel Berland, Henry Kennedy, and Colette Dehay. G1 phase regulation, area-specific cell cycle control, and cytoarchitectonics in the primate cortex. *Neuron*, 47(3):353–364, August 2005. ISSN 0896-6273. doi: 10.1016/j.neuron.2005.06.032. URL http://www.ncbi.nlm.nih.gov/pubmed/16055060. PMID: 16055060.

[69] J. L. Sherley, P. B. Stadler, and J. Scott Stadler. A quantitative method for the analysis of mammalian cell proliferation in culture in terms of dividing and non-dividing cells. *Cell Proliferation*, 28:137–144, March 1995. ISSN 0960-7722, 1365-2184. doi: 10.1111/j.1365-2184.1995.tb00062.x. URL http://doi.wiley.com/10.1111/j.1365-2184.1995.tb00062.x.

[70] Mariana Gabi, Christine E. Collins, Peiyan Wong, Laila B. Torres, Jon H. Kaas, and Suzana Herculano-Houzel. Cellular scaling rules for the brains of an extended number of primate species. *Brain, Behavior and Evolution*, 76:32–44, 2010. ISSN 1421-9743, 0006-8977. doi: 10.1159/000319872. URL http://www.karger.com/doi/10.1159/000319872.

[71] Herculano-Houzel. Coordinated scaling of cortical and cerebellar numbers of neurons. *Frontiers in Neuroanatomy*, 4(12), 2010. ISSN 16625129. doi: 10.3389/fnana.2010.00012. URL http://www.frontiersin.org/neuroanatomy/10.3389/fnana.2010.00012/abstract.

[72] Suzana Herculano-Houzel. Not all brains are made the same: new views on brain scaling in evolution. *Brain, Behavior and Evolution*, 78(1):22–36, 2011. ISSN 1421-9743. doi: 10.1159/000327318. URL http://www.ncbi.nlm.nih.gov/pubmed/21691045. PMID: 21691045.

[73] M J Burek and R W Oppenheim. Programmed cell death in the developing nervous system. *Brain Pathology*, 6(4):427–446, October 1996. ISSN 1015-6305. URL http://www.ncbi.nlm.nih.gov/pubmed/8944315. PMID: 8944315.

[74] J B Hutchins and S W Barger. Why neurons die: cell death in the nervous system. *The Anatomical Record*, 253(3):79–90, June 1998. ISSN 0003-276X. URL http://www.ncbi.nlm.nih.gov/pubmed/9700393. PMID: 9700393.

[75] Fabiana Bandeira, Roberto Lent, and Suzana Herculano-Houzel. Changing numbers of neuronal and non-neuronal cells underlie postnatal brain growth in the rat. *Proceedings of the National Academy of Sciences of the United States of America*, 106(33):14108–14113, August 2009. ISSN 1091-6490. doi: 10.1073/pnas.0804650106. URL http://www.ncbi.nlm.nih.gov/pubmed/19666520. PMID: 19666520.

[76] K Zilles, E Armstrong, A Schleicher, and H J Kretschmann. The human pattern of gyrification in the cerebral cortex. *Anat. Embryol.*, 179(2):173–179, 1988. ISSN 0340-2061. PMID: 3232854.

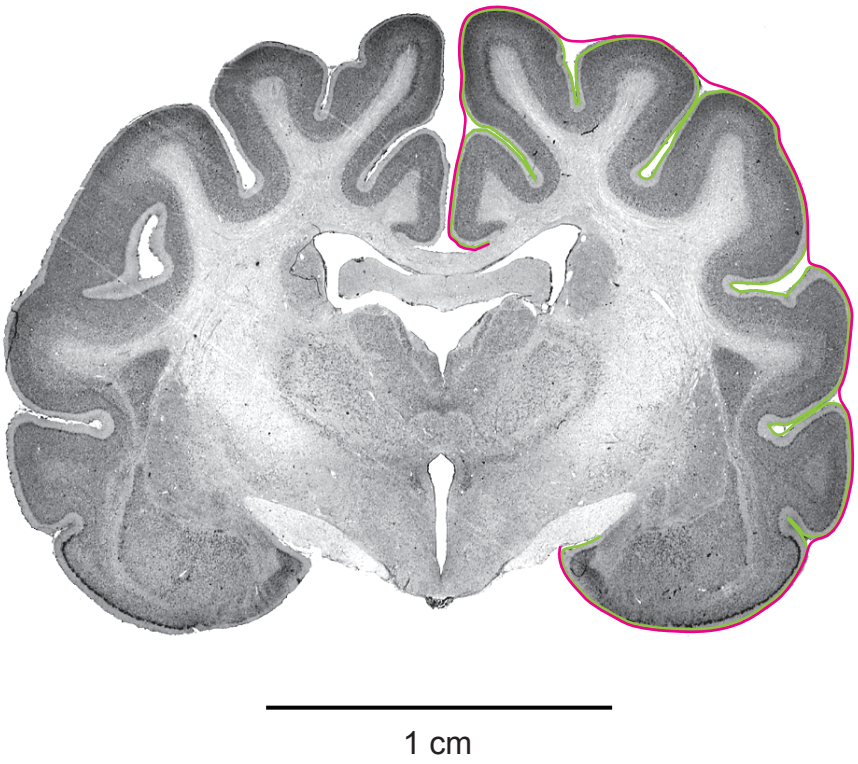

Figure S1: Coronal section of the brain of an adult house cat (*Felis catus*) (obtained from www.brainmuseum.org) illustrating the method used to calculate GI values as described in [76]. Green line, actual contour; magenta line, hypothetical outer contour.

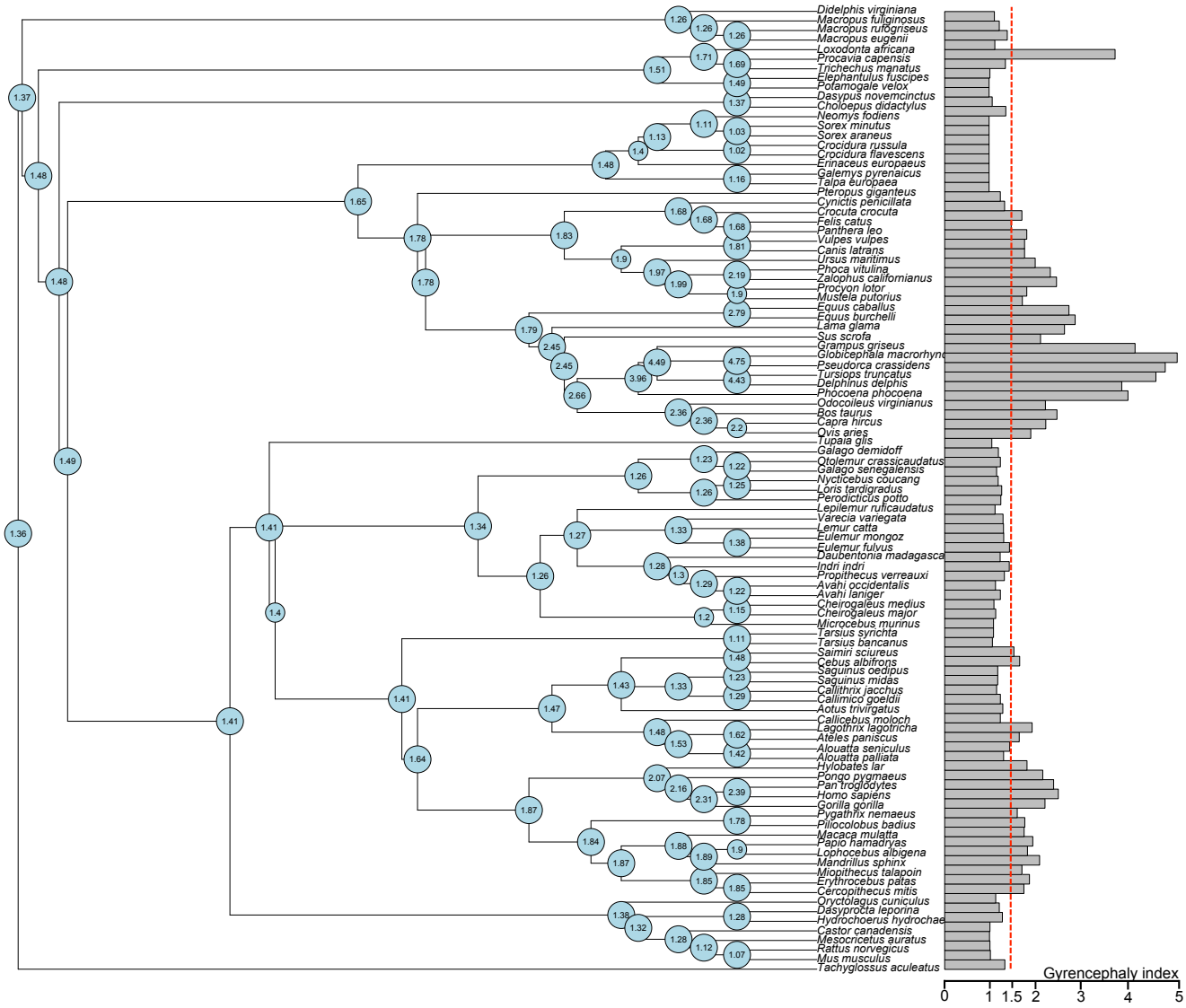

Figure S2: Maximum-likelihood ancestral node reconstruction of GI values at all internal nodes based on a delta ($\delta = 2.635$) selection model. Barplot shows the distribution of GI values across the phylogeny; dashed red line indicates GI = 1.5.

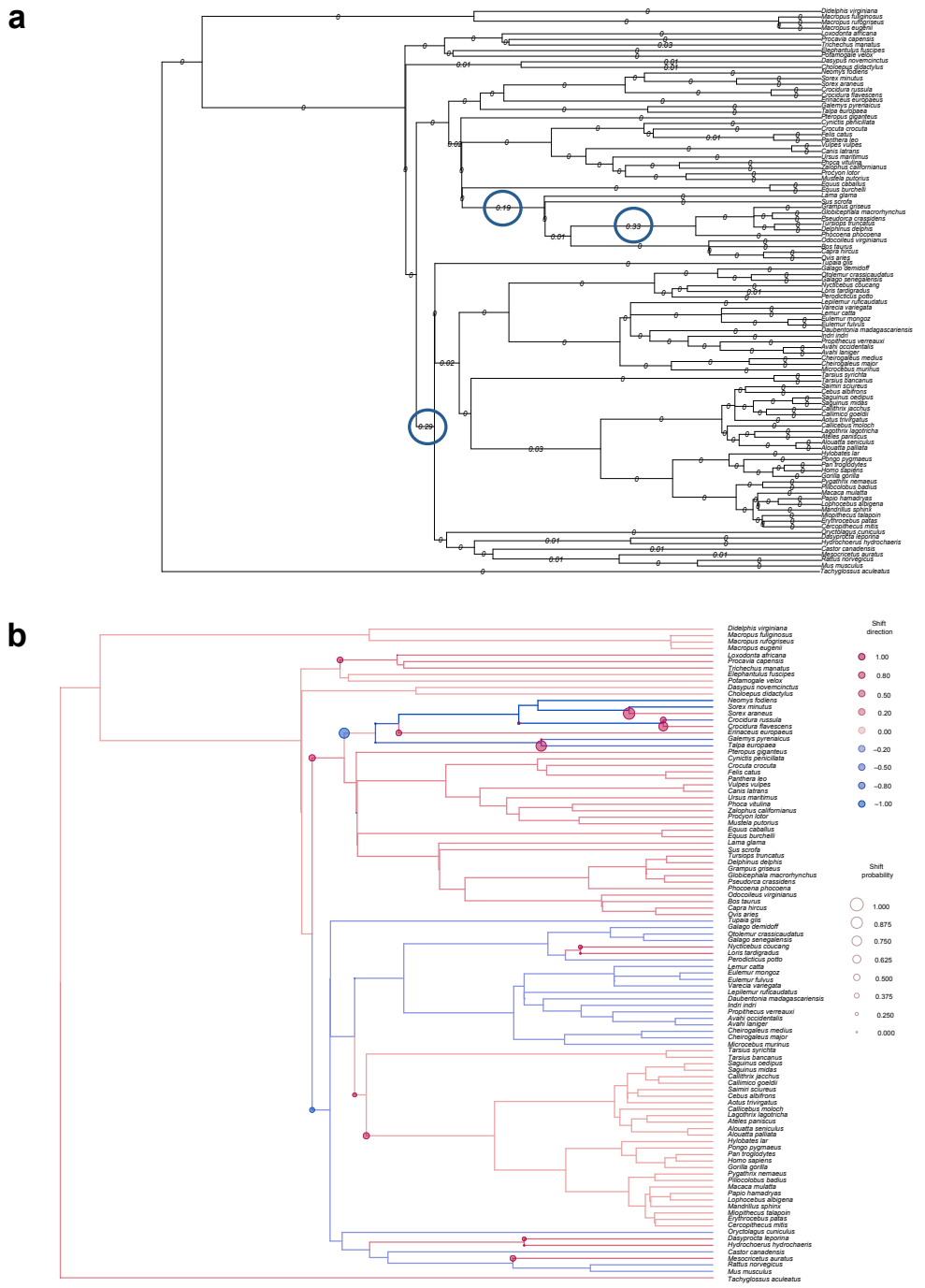

Figure S3: Rate-transitions in the mutation rate of GI values along lineages of the mammalian phylogeny (a) A two-mode selection model that weights low over high root-to-tip substitutions. Numbers on the branches indicate the change in mutation-rate compared to the previous branch; 0 values indicate no significant change, values > 0 indicate significant change ($P < 0.05$). Note the especially high rate-transitions leading to primates, cetartiodactyls, and cetaceans (open blue circles). (b) Mutation- and transition-rate estimates of GI values using an Ornstein-Uhlenbeck selection model. Branches are colored to illustrate whether the mutation-rate estimates along each lineage are above (red) or below (blue) the median rate (orange); nodes are circled to indicate the posterior support of a transition-rate-shift event. The gradient of colors (see key) indicates the degree of deviation of the mutation-rate estimates (branches) and transition-rate estimates (nodes) from the median, with the highest deviation being arbitrarily set to $\pm$ 1.0 and the median to 0.0; the size of the circles (see key) at the nodes indicates the degree of posterior support for a transition-rate-shift event, with the highest value being arbitrarily set to 1.0 and lack of support to 0.0. Note that simians have evolved GI values at a rate consistent with the mammalian median.

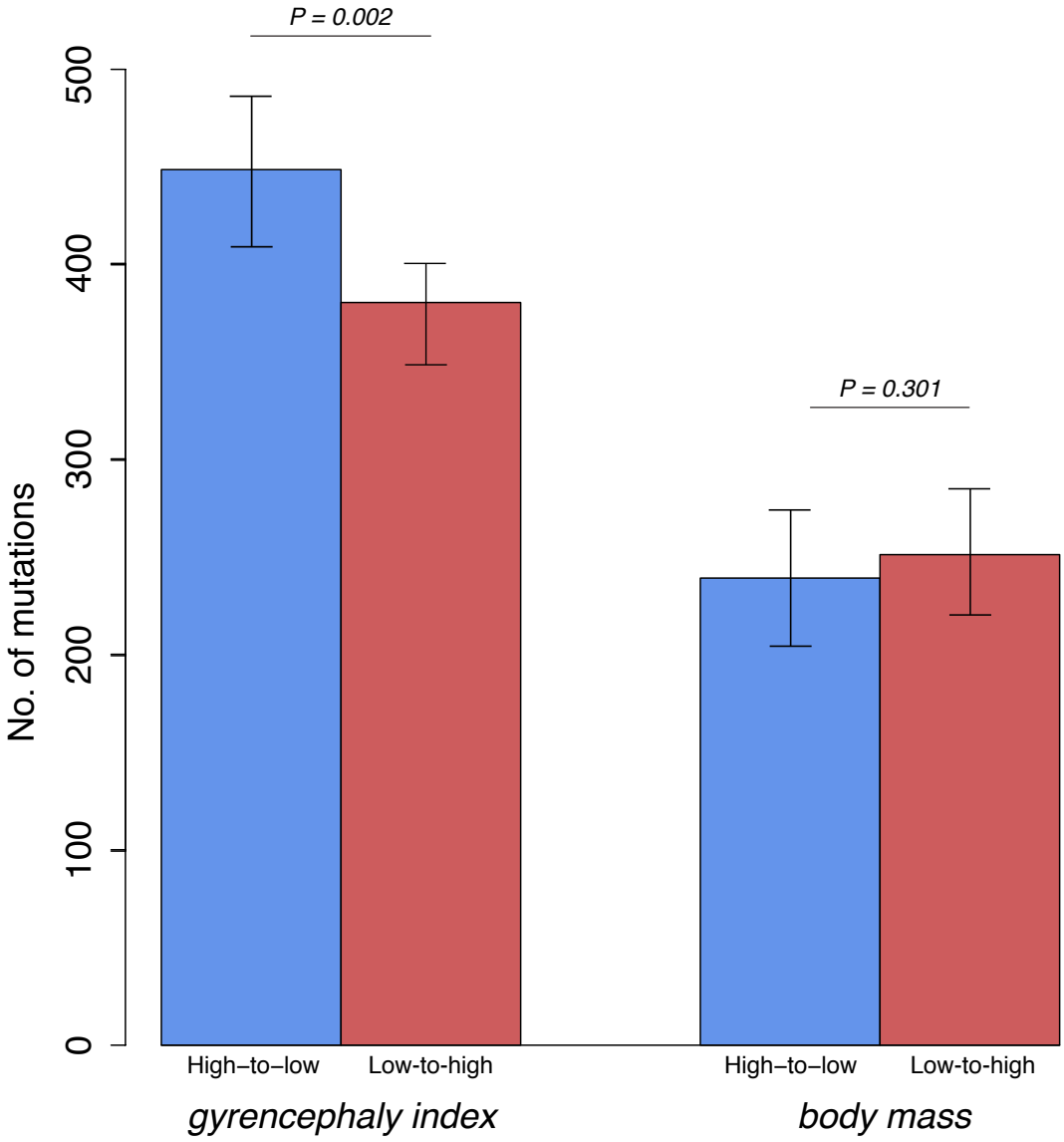

Figure S4: Barplots of types of transitions over mammalian evolution between four GI groups (see Fig. 2a) and between five body mass groups averaged over 105 simulations. The number of total transitions from one GI or body mass group to another is summed as either high-to-low or low-to-high transitions. Note that significantly more high-to-low than low-to-high transitions are observed for GI, but that no significant difference in type of transition is observed for body mass.

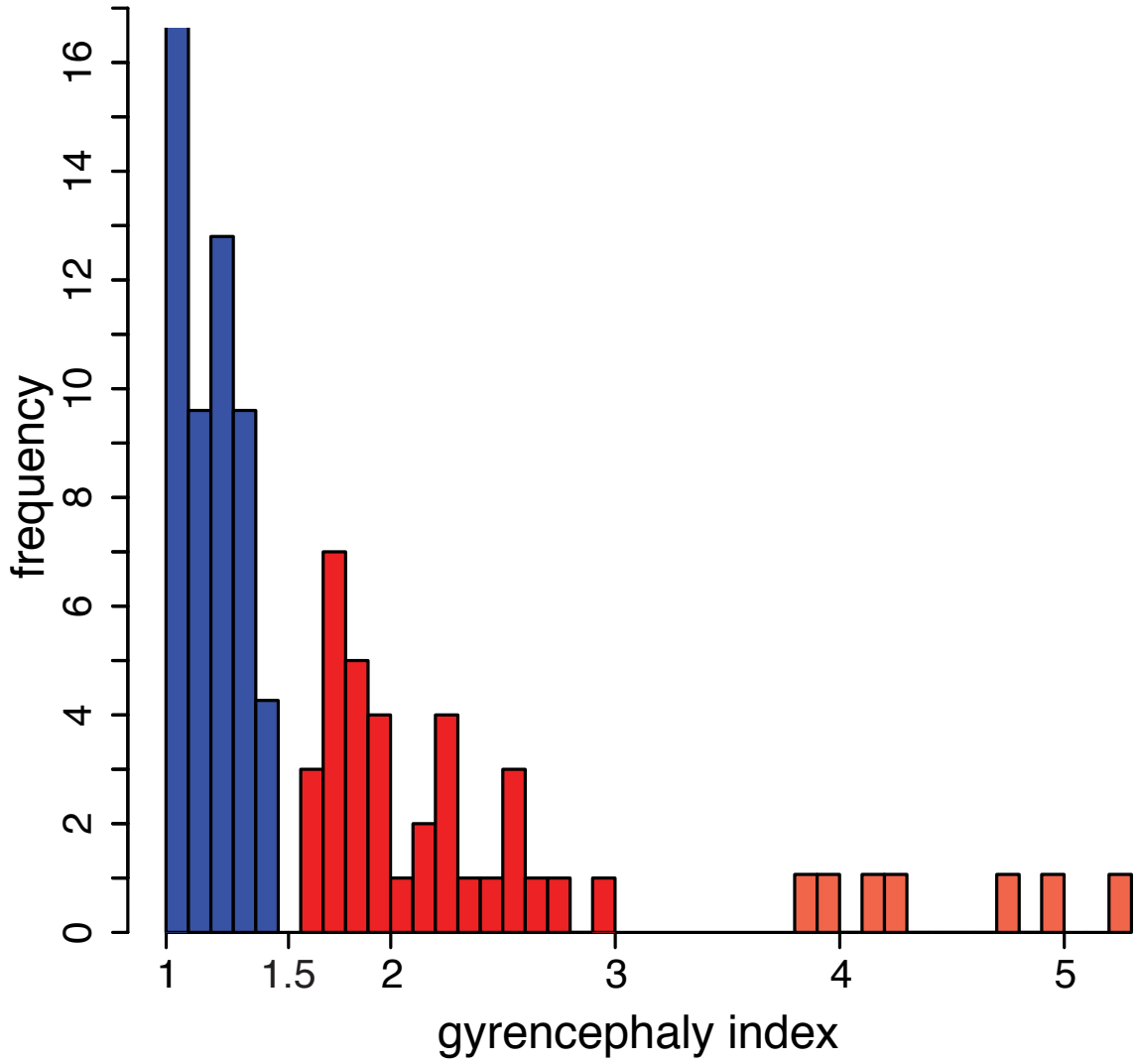

Figure S5: The bimodal distribution of GI values across the phylogeny is non-random. A histogram showing the frequency of occurrence of GI values, binned at 0.05 intervals, for the 102 mammalian species listed in Table S1. Blue, GI values ≤ 1.5; red, GI values > 1.5. The bimodal distribution of GI values shows a natural break at GI $= 1.5$, which is supported by energy-based hierarchical clustering (see Fig. 2b). Note the possibility for a third GI group (GI > 3, tomato red), constituting cetaceans and elephant; however, we have too few sampled species from these orders to assess the group decisively.

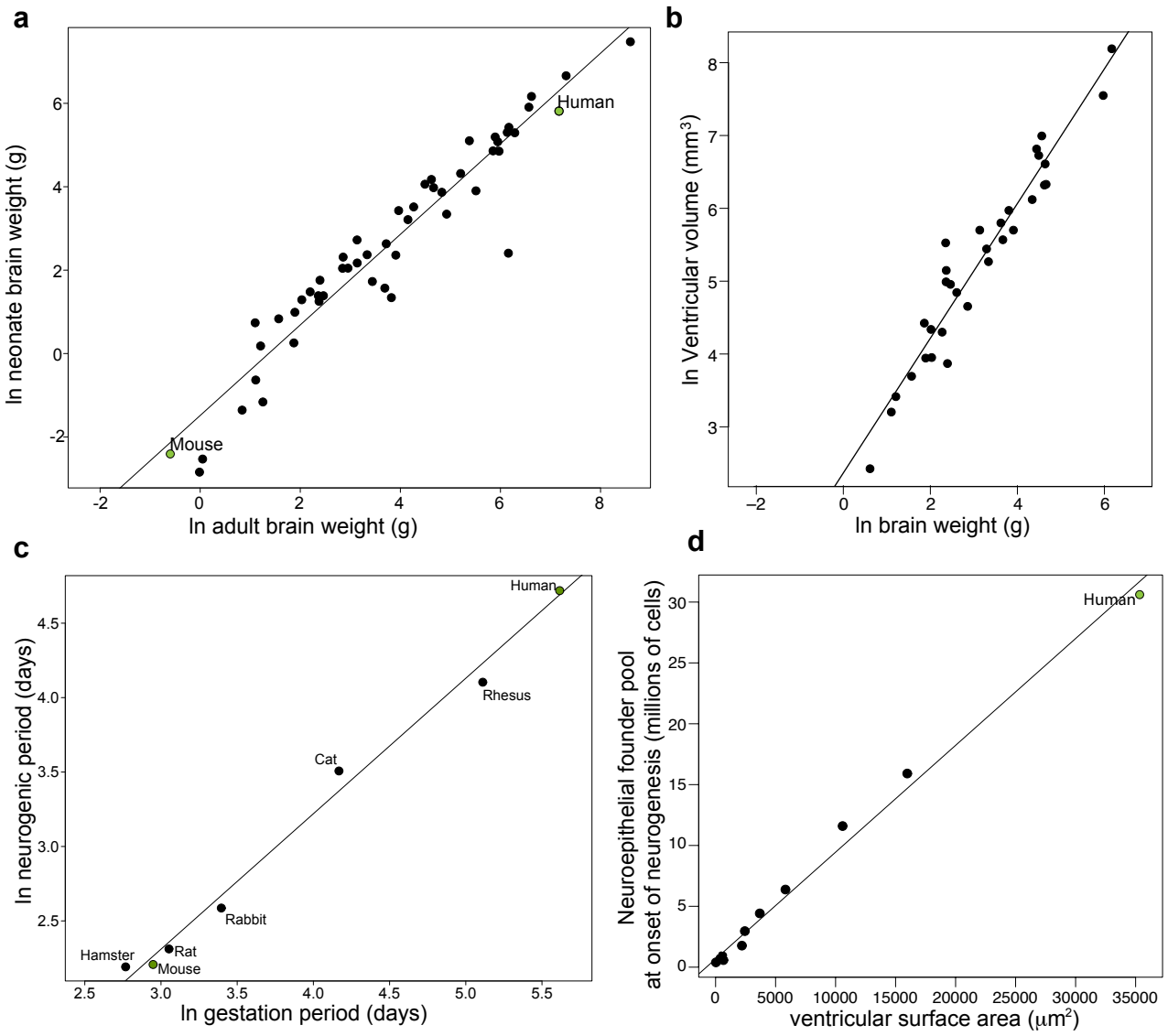

Figure S6: Ln-transformed plots of neonate brain weight (a) and ventricular volume (b) as functions of adult brain weight, neurogenic period as a function of gestation period (c); and a plot of neuroepithelial founder cells as a function of ventricular surface area (d).(a) Neonate brain weight scales linearly with adult brain weight for 52 eutherian species ($y = 1.09x - 1.49$, $R^2 = 0.92$, $P = 6 \times 10^{-7}$). (b) Ventricular volume scales linearly with adult brain weight for 30 eutherian species ($y = 0.93x + 2.37$, $R^2 = 0.93$, $P = 9 \times 10^{-8}$). (c) Neurogenic period scales linearly with gestation period for a sample of six species ($y = 0.91x - 0.42$, $R^2 = 0.94$, $P = 0.0002$), spanning two mammalian superorders. Predicted neurogenic period is shown for human. (d) Ventricular surface area, converted from ventricular volume (see Methods), scales linearly with our estimated neuroepithelial founder populations ($y = 6.7 \times 10^5 + 878x$, $R^2 = 0.94$, $P = 5 \times 10^{-8}$). (a, c) Note that these plots demonstrate the strong predictive powers of adult brain weight and gestation period for neonate brain weight and neurogenic period, respectively, validating the assumptions made in Fig. 4.

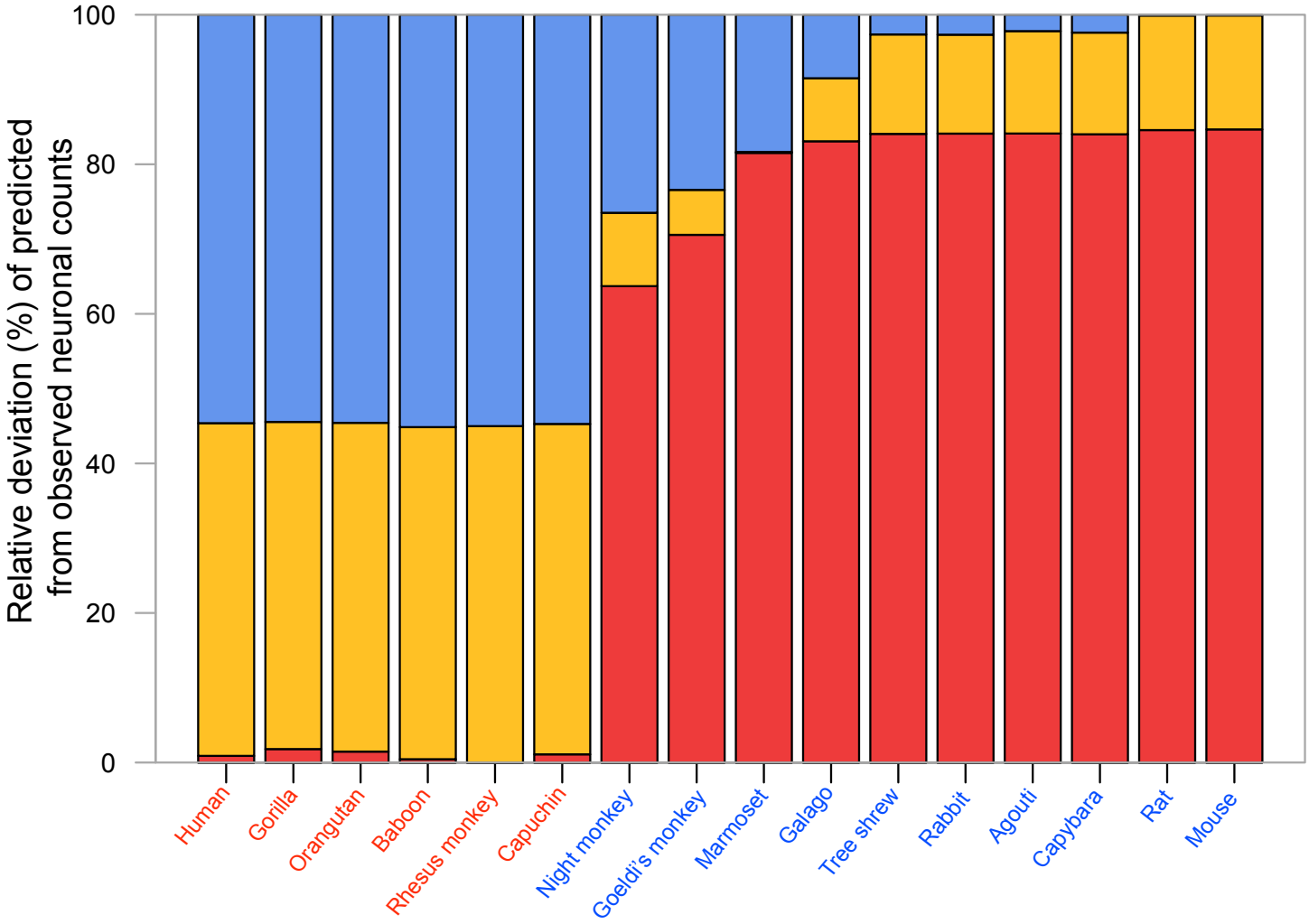

Figure S7: Stacked barplot, for the indicated species, of deviations between the observed neocortical neuron counts and the ones predicted based on human (red), mouse (blue) and marmoset (yellow) lineage combinations (see Table 2 and Fig. 5). For each species, deviations were calculated as |100*((Predicted Observed)/Observed)| and then divided by the sum of deviations obtained for all three lineage combinations. Note that predictions based on the marmoset lineage combination deviate from observed neuron counts not only for the 6 species with a GI value > 1.5 (red text), but also for 8 of the 10 species with a GI ≤ 1.5 (blue text), indicating a necessity for differential proportional occurrences of bRG in low-GI species.

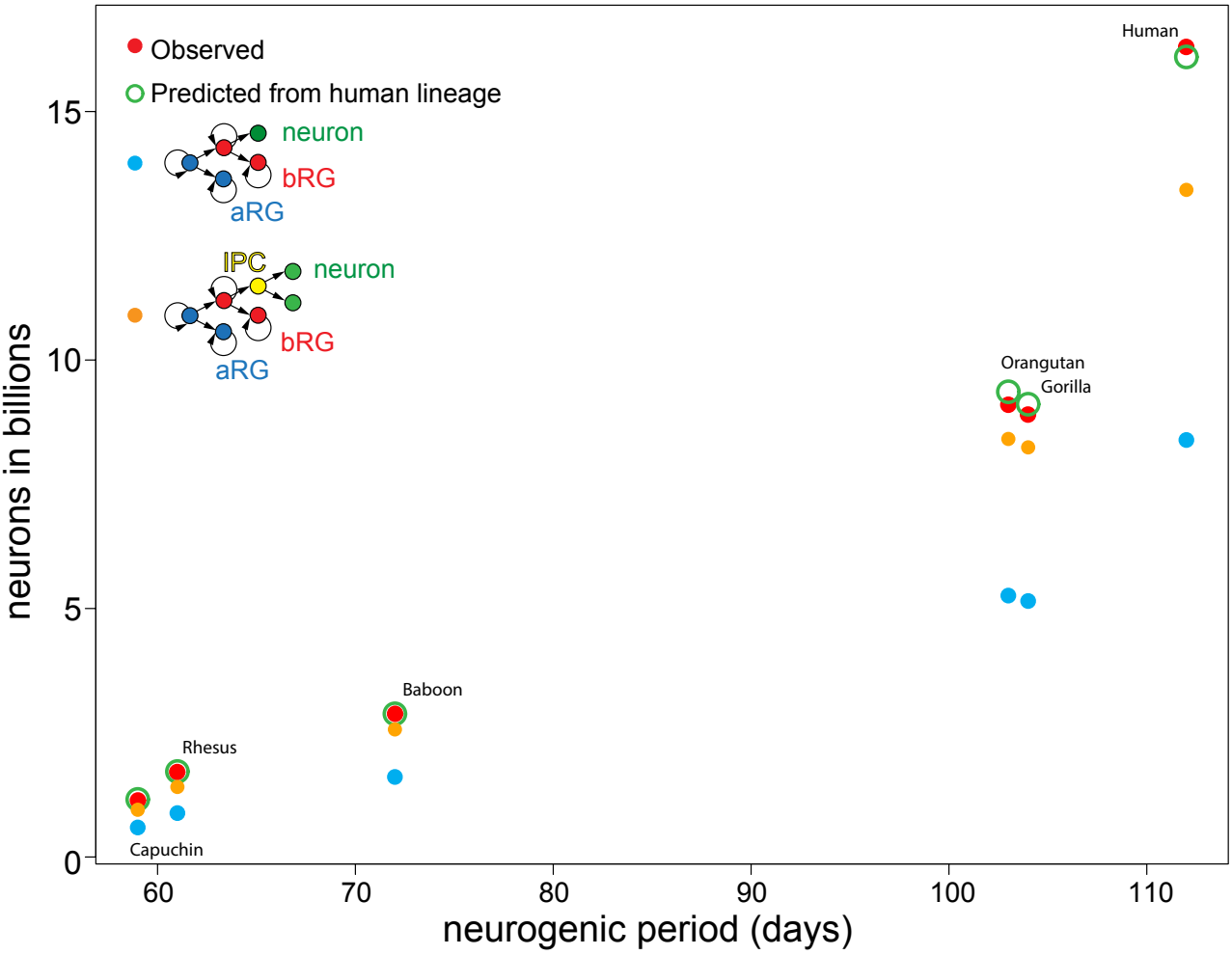

Figure S8: Plot of observed neocortical neuronal count (red circles) as a function of neurogenic period for six species with a GI value > 1.5. Predicted neuron counts are presented for the human lineage combination (green circles; see Fig. 5, Table 2) and for two further lineages, each of which is assumed to have a 100% proportional occurrence: direct neurogenesis from bRG (blue circle) and indirect neurogenesis from bRG via a self-consuming IP cell (orange circle). Note that indirect neurogenesis from bRG via IPs is nearly sufficient to achieve the observed neuronal count in the Capuchin monkey.

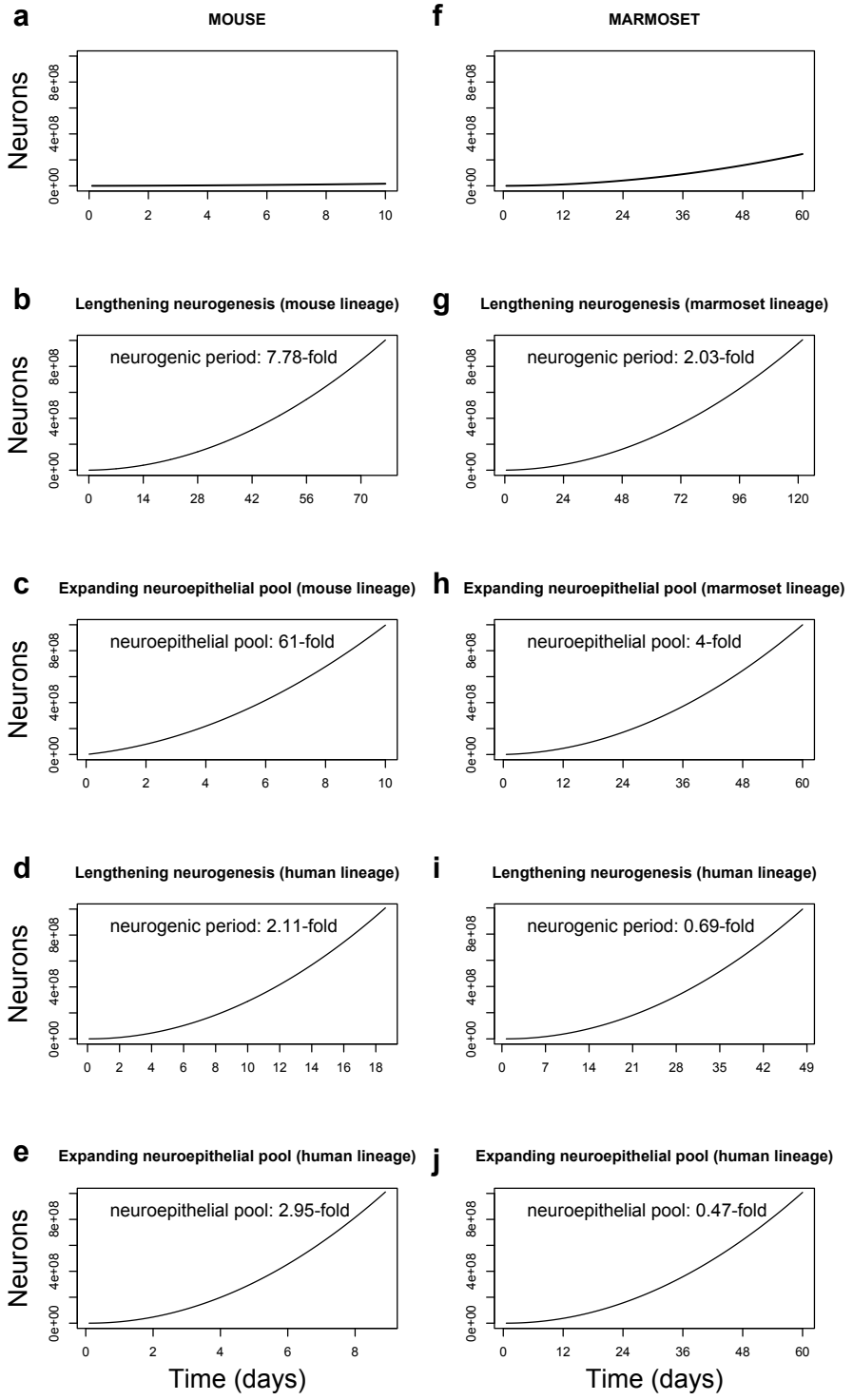

Figure S9: Calculating the adaptiveness of bRG-derived TAPs in mouse (a-e) and marmoset (f-j) in achieving 10^9 neurons with respect to lengthening neurogenic period and expanding neuroepithelial founder pool size. The fold-change of lengthening neurogenic period or expanding neuroepithelial founder pool size is indicated in each relevant plot. (a) The observed neurogenic period and founder pool size in mouse generates 1.37 x 10^7 neurons using the mouse lineage combination. (b, c) Lengthening the neurogenic period (b) or expanding the founder pool size (c) using the mouse lineage combination to achieve 10^9 neurons. (d, e) Lengthening the neurogenic period (d) or expanding the founder pool size (e) using the human lineage combination to achieve 10^9 neurons. (f) The observed neurogenic period and founder pool size in marmoset generates 2.45 x 10^8 neurons using the marmoset lineage combination. (g, h) Lengthening the neurogenic period (g) or expanding the founder pool size (h) using the marmoset lineage combination to achieve 10^9 neurons. (i, j) Lengthening the neurogenic period (i) or expanding the founder pool size (j) using the human lineage combination to achieve 10^9 neurons.

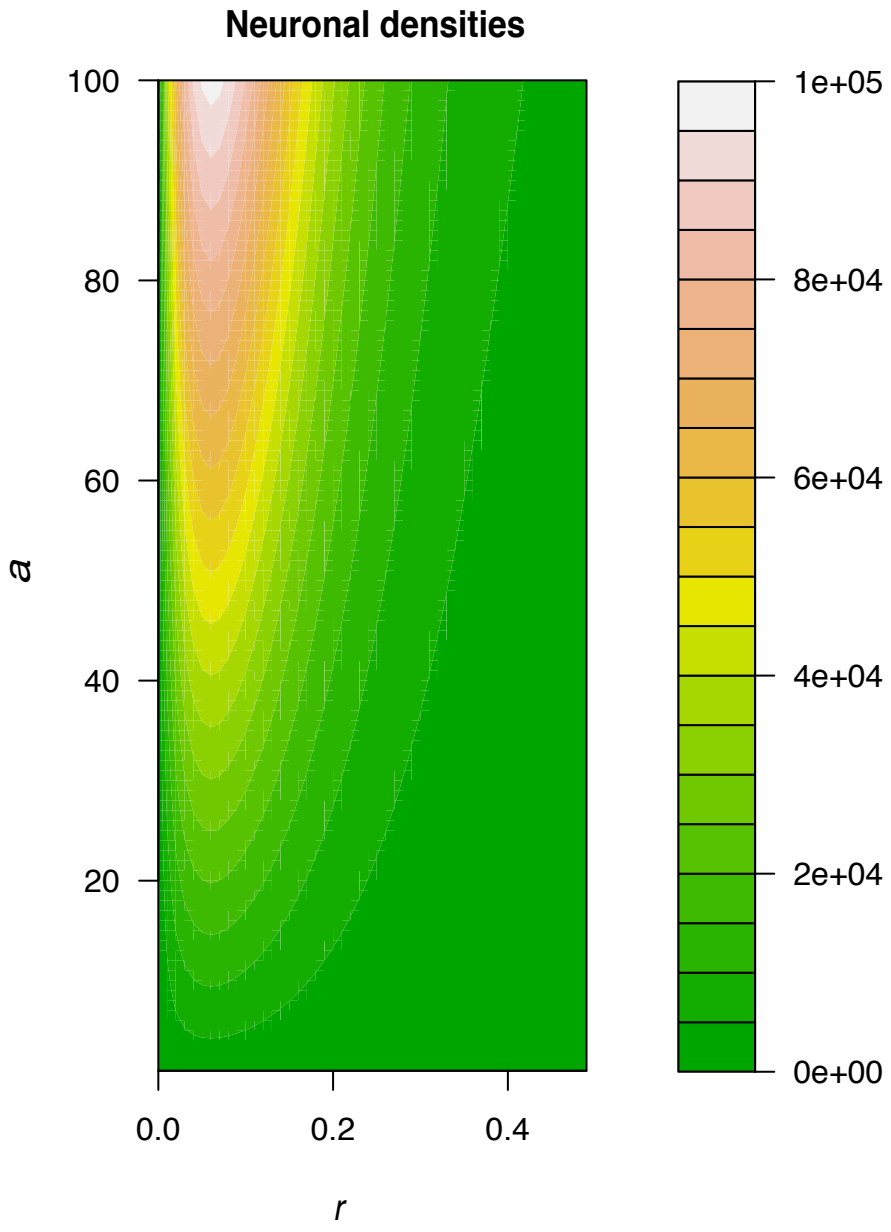

Figure S10: Neuronal outputs from solutions to ODEs describing direct versus indirect neurogenesis for growth-rate values $\leq$ 0.5. Contour plot of neuronal densities for a varying initial asymmetrically dividing cell population (a) and likelihood of direct ($r = 1$) versus indirect ($r = 0$) neurogenesis. Note that neuronal output increases maximally when both the initial cell pool increases ($a \to 100$) and the likelihood of indirect neurogenesis increases ($r \to 0$).